

Analytical Solution of Spinning, Eccentric Binary Black Hole Dynamics at the Second Post-Newtonian Order

Tom Colin,^{1,*} Sashwat Tanay,^{1,2,†} and Laura Bernard^{1,‡}

¹*Laboratoire d'étude de l'Univers et des phénomènes eXtrêmes (LUX), Observatoire de Paris, Université PSL, Sorbonne Université, CNRS, 92190 Meudon, France*

²*Universidad de Ingeniería y Tecnología – UTEC, Jr. Medrano Silva 165 - Barranco 15063, Lima, Peru*

Recent gravitational wave (GW) detections showing signatures of eccentricity and spin precession underscore the need to model binary black holes (BBHs) possessing these features simultaneously. Most efforts over the past fifteen years to model spinning BBHs and their corresponding GWs have relied on heuristically twisting waveforms from non-precessing systems. This approach is based on empirical observations rather than first principles. This article aims to model the GWs from spinning and eccentric BBHs from a first-principles approach within general relativity and post-Newtonian (PN) approximation. Building on the already-existing 1.5 PN solution, we construct an analytical solution for the time evolution of the relative separation vector, the individual black hole spin vectors, and the orbital angular momentum vector at 2PN order for BBHs with arbitrary spins and eccentricity. Such a solution is not fully 2PN accurate in that the tiny orbital timescale fluctuations in the solutions for the spins are only leading 1.5PN order accurate, instead of 2PN. However, it is shown that our new 2PN solution is still an order of magnitude improvement over the earlier 1.5PN solution, underlining the sub-dominant nature of the neglected next-to-leading-order oscillations in the spin solutions.

1. INTRODUCTION

Gravitational wave (GW) science has entered the era of precision astronomy. The advent of the next generation of gravitational wave detectors, such as Einstein Telescope and the space-based LISA interferometer will introduce significant data analysis challenges if we wish to extract the maximal scientific return from observations. To achieve this goal, a key requirement is the ability to model all possible binary systems of interest with very high precision.

Following many GW detections that carry signatures of spinning or eccentric black holes (BHs) [1–3], the interest in the GW community is converging towards such systems. BBHs with spins or eccentricity are considered interesting because their detection sheds light over the astrophysical environment where these systems evolved and merged (isolated or dynamical formation channels, chemically homogeneous formation, supernova kicks, hierarchical merger or merger inside active galactic nuclei) [4–6]. Just as interesting is the interplay between the spins and the eccentricities. While there is a danger that the two properties can mimic each other, leading to degeneracies [7, 8], there have also been efforts to make eccentricity detections sharper with the help of spin measurements [9, 10]. Given this interesting and treacherous terrain, it is desirable to construct from first principles, analytical solutions of the BBH orbital dynamics and the associated GWs. This is so because analytical solutions, although generally elusive, expose mathematical structures and relations between quantities to a greater degree than numerical or empirically constructed phenomenological ones. This gives hope to ameliorate the degeneracy issue between spins and eccentricity. Another aspect is the quick evaluation and implementation owing to the analytical nature of solutions.

Gravitational waveform modeling relies on different techniques to capture the distinct phases of compact binary coalescences. While numerical relativity is essential for the non-linear merger regime [11, 12] and black hole perturbation theory is used for the ringdown stage [13, 14], the post-Newtonian (PN) formalism remains the standard to determine the early inspiral dynamics [15]. The PN framework's analytic nature allows for rapid waveform generation across arbitrary parameter spaces, making it a key ingredient to generate full inspiral-merger-ringdown (IMR) models, including the effective-one-body (EOB) [16] and Phenom [17] classes of IMR waveforms.

To generate gravitational waveforms, one must first solve the equations of motion (EOMs), ideally using analytical methods, before using them to get the expressions for the energy, linear and angular momenta fluxes and the GW modes. In the absence of analytical orbital solutions for spinning BBHs, a certain “twist up” method has become the standard in the GW community [18–20]. It was empirically observed that GWs from spinning BBHs can be very well

* tom.colin@obspm.fr

† stanay@utec.edu.pe

‡ laura.bernard@obspm.fr

approximated by applying certain time-dependent rotation¹ on GWs originating from non-precessing BBHs with the help of Wigner matrices. Various GW models have been built adopting this approach; the state-of-the-art includes both eccentricity and spin simultaneously [21–23].

On the other hand, the construction of GWs from first principles for spinning BBHs has been stalled for a long time due to the unavailability of orbital and spin solutions for precessing and eccentric BBHs. The standard framework for solving the dynamics of non-spinning systems has been the quasi-Keplerian parametrization (QKP). Originally established by Damour and Deruelle [24] for the 1PN dynamics, it has been successfully generalized to 4PN order in the non-spinning sector [25, 26] and to 3PN for aligned-spin configurations [27, 28]. However, while these standard parametrizations are typically derived via an analytical integration of the EOMs, the inclusion of precessing 2PN spin–spin effects renders analytical integration difficult.

The goal of the present work is to address this challenge by providing an analytical solution $(\mathbf{R}(t), \mathbf{S}_1(t), \mathbf{S}_2(t), \mathbf{L}(t))$ for the orbital and spin motions for precessing, eccentric BBHs at 2PN order. Before going to the core of the work, in the following subsection, we review previous attempts to solve the problem, highlighting their respective contributions and limitations. We end the introduction by further motivating our work with respect to these previous attempts and by providing an executive summary of the results obtained.

A. Previous analytical solutions

The development of analytical solutions for the relative separation \mathbf{R} and the angular momenta \mathbf{L} , \mathbf{S}_1 , and \mathbf{S}_2 for spinning binaries on eccentric orbits has proceeded step by step, with different works addressing various sectors of the 2PN dynamics. Below, we review the key results that provide the foundation for the present work.

Non-spinning 2PN dynamics: The 1PN solution was first proposed by Wagoner and Will in 1976 [29]. Thereafter, the quasi-Keplerian parametric solution for the relative separation \mathbf{R} in non-spinning binaries was originally established by Damour and Deruelle at 1PN order [24] and extended to 2PN by Wex and Schäfer [30]². Working with the Arnowitt-Deser-Misner (ADM) [33] Hamiltonian, they derived the explicit expressions for the radial coordinates and the orbital phase through analytical integration of the EOMs. A defining feature of the non-spinning conservative dynamics is the conservation of the direction of the orbital angular momentum, which restricts the motion to a fixed plane. However, unlike in Newtonian gravity, the orbits are not closed ellipses; they exhibit a relativistic periastron advance, characterised by the quantity k . Consequently, the radial and angular motions decouple, necessitating distinct eccentricity parameters (e_r, e_t, e_ϕ) to describe respectively the radial separation, the time evolution (generalized Kepler equation) and the orbital phase. At 2PN order, this formalism preserves the functional form of the Keplerian solution but introduces additional periodic corrections proportional to the higher harmonics of the eccentric anomaly. This framework forms the foundation upon which spin effects can be incorporated.

Spin-orbit dynamics at 1.5PN: The first complete analytical solution incorporating spin-orbit couplings on eccentric orbits was provided by Cho and Lee [34] at leading (1.5PN) order in the spin sector, while ignoring the 1PN terms in the Hamiltonian. Using the ADM Hamiltonian with the Newton-Wigner-Pryce (NWP) spin supplementary condition, they derived closed-form expressions for all three angular momentum vectors \mathbf{L} , \mathbf{S}_1 , and \mathbf{S}_2 in terms of elliptic integrals. Cho and Lee also provided the QKP for the orbital motion. The radial coordinate $R(t)$ retains the same functional form as the 1PN non-spinning parametrization of Damour and Deruelle [24], while the azimuthal angle $\phi(t)$ extends the 1PN expression through additional terms involving incomplete elliptic integrals of the third kind. These elliptic contributions capture the precession of the orbital plane induced by spin-orbit coupling. Ref. [35] subsequently completed this 1.5PN solution by incorporating the 1PN non-spinning orbital corrections that were initially omitted by Cho and Lee.

Orbit-averaged 2PN spin dynamics: The inclusion of 2PN spin-spin interactions makes the obtention of full 2PN analytical solutions very hard. To overcome this difficulty, orbit averaging has been used in the past. Orbit averaging filters out the tiny and short orbital timescale oscillations that the full solution possesses, thereby simplifying the EOMs, and making the construction of the full solution possible. The orbit-averaged EOMs at 2PN were first worked out by Schnittman in Ref. [36]. Racine identified a new constant of motion for these EOMs, which ultimately led to the construction of the full solution in Refs. [21, 37, 38]. Note that the unaveraged solutions at 1.5PN of Refs. [34, 35] do contain these tiny oscillations.

Another interesting development was the discovery of the 2PN constants of motion in Ref. [39] for the full 2PN EOMs, thereby establishing its 2PN perturbative integrability. As Racine’s constant of motion [40] helped construct

¹ This rotation approximately tracks the orbital angular momentum.

² Although it is not useful for the present work, the QKP for non-spinning eccentric binaries has successively been extended to 3PN and 4PN orders [31, 32].

the exact solution for 2PN orbit-averaged EOMs, we will use the 2PN unaveraged constant of motion to construct our solution in later sections.

2PN spin effects in orbital motion. Gergely [41] and later Klein and Jetzer [42] worked out the solution for the magnitude of the orbital position vector at 2PN order including both spin-orbit and spin-spin effects. Working in harmonic coordinates with Kidder’s Lagrangian formulation [43], Ref. [42] adopted a spin supplementary condition different from the NWP spin supplementary condition used in the ADM approach³.

B. Motivation and scope of the present work

When it comes to solving the dynamics of BBHs with arbitrary spins and eccentricity, the current state of the art is the solution presented in Refs. [34, 35], which is valid at 1.5PN order⁴. This paper is an attempt to extend the solution to 2PN order with the ADM Hamiltonian and NWP spin supplementary condition.

Our calculations can broadly be divided into two parts. First, Sections 3B–3C deal with orbital and spin angular momenta (\mathbf{L} , \mathbf{S}_1 , and \mathbf{S}_2). There, we construct a solution that goes beyond orbit-averaging by hybridizing the 1.5PN solution of Ref. [35] with the 2PN orbit-averaged solution of Ref. [21]. The resulting hybrid solution has tiny orbital time-scale variations which are washed away during the process of averaging while constructing the orbit-averaged solution. Such solution may be called “nearly 2PN accurate” since the missing 2PN oscillations are sub-dominant when compared to the other 2PN effect that we do account for.

After having tackled the angular momenta, in Section 4, taking inspiration from the ansatz-based approach of Klein and Jetzer [42], we construct the solution of position vector magnitude $R(t)$ and phase $\phi(t)$ in a non inertial frame centered on \mathbf{L} . While these expressions are themselves 2PN accurate, the final determination of the position vector \mathbf{R} is again only “nearly 2PN accurate”. This is due to the fact that the definition of ϕ hinges on the definition of \mathbf{L} , which require using our hybrid 2PN solution.

The analytical solutions derived in this work have been implemented in a *Mathematica* notebook, `2PN_BBH_solution.nb`, which is available in a public GitHub repository [45].

C. Notation and Conventions

Mass parameters— We consider a binary system with individual masses $m_1 > m_2$, total mass $m = m_1 + m_2$, reduced mass $\mu = m_1 m_2 / m$, and symmetric mass ratio $\nu = \mu / m$. We further define the auxiliary mass-weighted parameters $\delta_a = 2\nu(1 + 3m_b/4m_a)$ and $\sigma_a = \nu(1 + m_b/m_a)$, with indices $(a, b) \in \{(1, 2), (2, 1)\}$.

Orbital variables— We work in the center-of-mass frame and employ reduced variables, denoted by lowercase letters. The relative separation vector is rescaled by the total mass, $\mathbf{r} = \mathbf{R}/(Gm)$, while the canonical momentum is rescaled by the reduced mass, $\mathbf{p} = \mathbf{P}/\mu$. The coordinate time is rescaled as $t = t'/(Gm)$, where t' is the physical time. Overdots denote derivatives with respect to this reduced time, $\dot{x} \equiv dx/dt$. The unit separation vector is $\mathbf{n} = \mathbf{r}/r$, with $r = \|\mathbf{r}\|$. We describe the dynamics using the reduced Hamiltonian $h = H/\mu$.

Angular momenta— The reduced orbital angular momentum is defined as $\mathbf{l} = \mathbf{r} \times \mathbf{p}$. The individual spin vectors are also rescaled by μGm , such that $\mathbf{s}_a = \mathbf{S}_a/(\mu Gm)$. The total reduced angular momentum is $\mathbf{j} = \mathbf{l} + \mathbf{s}_1 + \mathbf{s}_2$. We characterize the spin interactions using two specific linear combinations: the effective spin $\mathbf{s}_{\text{eff}} = \delta_1 \mathbf{s}_1 + \delta_2 \mathbf{s}_2$ and the auxiliary vector $\mathbf{s}_0 = \sigma_1 \mathbf{s}_1 + \sigma_2 \mathbf{s}_2$.

Conventions— In this work, the post-Newtonian (PN) order is defined by the scaling parameter $x_{\text{PN}} \equiv 1/(c^2 r_p)$, where r_p is the reduced relative separation at periastron. An n PN correction scales as x_{PN}^n . Finally we set $G = 1$ throughout this work.

2. HAMILTONIAN FORMULATION

A. The 2PN spinning Hamiltonian

We consider a BBH system consisting of two spinning black holes with masses m_1 and m_2 in a bound orbit around their common center of mass. The dynamics of the system is governed by a Hamiltonian expressed in ADM [33] with

³ As demonstrated by Barker and O’Connell [44], different spin supplementary conditions correspond to different choices of the center-of-mass location and are related by coordinate transformations; they represent physically equivalent descriptions.

⁴ The solution of Ref. [42] does not track the precession of the orbital angular momentum relative to the inertial frame, leading to ambiguities in the definition and evolution of the orbital phase ϕ .

the NWP spin supplementary condition [46, 47], which fixes the center-of-mass worldline of each spinning body. The (reduced) Hamiltonian reads⁵ [48–51]

$$h = h_N + \frac{1}{c^2} h_{1\text{PN}} + \frac{1}{c^2} h_{\text{SO}} + \frac{1}{c^4} h_{2\text{PN}} + \frac{1}{c^2} h_{\text{SS}}, \quad (2.1)$$

where

$$h_N = \frac{p^2}{2} - \frac{1}{r}, \quad (2.2a)$$

$$h_{1\text{PN}} = \frac{3\nu - 1}{8} p^4 - \frac{1}{2r} [(3 + \nu)p^2 + \nu(\mathbf{n} \cdot \mathbf{p})^2] + \frac{1}{2r^2}, \quad (2.2b)$$

$$h_{\text{SO}} = \frac{\mathbf{l} \cdot \mathbf{s}_{\text{eff}}}{r^3}, \quad (2.2c)$$

$$h_{2\text{PN}} = \frac{1 - 5\nu + 5\nu^2}{16} p^6 + \frac{1}{8r} [(5 - 20\nu - 3\nu^2)p^4 - 2\nu^2(\mathbf{n} \cdot \mathbf{p})^2 p^2 - 3\nu^2(\mathbf{n} \cdot \mathbf{p})^4] \\ + \frac{1}{2r^2} [3\nu(\mathbf{n} \cdot \mathbf{p})^2 + (5 + 8\nu)p^2] - \frac{1 + 3\nu}{4r^3}, \quad (2.2d)$$

$$h_{\text{SS}} = \frac{\nu}{r^3} \left[3(\mathbf{s}_1 \cdot \mathbf{n})(\mathbf{s}_2 \cdot \mathbf{n}) - \mathbf{s}_1 \cdot \mathbf{s}_2 + \frac{m_2}{2m_1} (3(\mathbf{s}_1 \cdot \mathbf{n})^2 - s_1^2) + \frac{m_1}{2m_2} (3(\mathbf{s}_2 \cdot \mathbf{n})^2 - s_2^2) \right]. \quad (2.2e)$$

The terms h_N , $h_{1\text{PN}}$, and $h_{2\text{PN}}$ correspond, respectively, to the Newtonian, first post-Newtonian, and second post-Newtonian non-spinning contributions. Spin-orbit effects are encoded in h_{SO} , while h_{SS} accounts for the spin-spin interactions. Up to 2PN, there is no emission of gravitational waves and the system is therefore conservative.

For a Kerr black hole, the spin angular momentum is given by [15]

$$\mathbf{S}_a = \chi_a \frac{Gm_a^2}{c}, \quad (2.3)$$

where $|\chi_a| \leq 1$, with equality corresponding to a maximally spinning black hole. The implicit factor of $1/c$ hiding inside \mathbf{S}_a alters the PN power counting: as a consequence, the spin-orbit coupling formally enters at 1.5PN order, while the spin-spin coupling appears at 2PN order.

The equations of motion for any dynamical variable f are obtained from its Poisson bracket with the Hamiltonian

$$\frac{df}{dt} = \{f, H\}. \quad (2.4)$$

The fundamental Poisson bracket relations for the phase-space variables $(\mathbf{R}, \mathbf{P}, \mathbf{S}_1, \mathbf{S}_2)$ are [52]

$$\{R_i, P_j\} = \delta_{ij}, \quad (2.5a)$$

$$\{S_{ai}, S_{bj}\} = \delta_{ab} \epsilon_{ijk} S_{bk}, \quad (2.5b)$$

where δ_{ij} is the Kronecker delta, ϵ_{ijk} is the Levi-Civita symbol, and the indices $a, b \in \{1, 2\}$

label the two bodies while $i, j, k \in \{1, 2, 3\}$ label spatial components. Additionally, for functions f and g of phase-space variables, the Poisson brackets obey the antisymmetry property and the chain rule,

$$\{f, g\} = -\{g, f\}, \quad (2.6)$$

$$\{f, g(\mathbf{V})\} = \{f, \mathbf{V}\} \frac{\partial g}{\partial \mathbf{V}}. \quad (2.7)$$

Note that the chain rule allows us to compute the Poisson bracket of any function of the phase-space variables. Any other Poisson bracket not lying within the purview of Eqs. (2.5)–(2.7) simply vanishes.

⁵ The Hamiltonian implicitly assumes the plus signature $(-, +, +, +)$ for the spacetime metric.

B. Equations of motion for angular momenta

Using Eqs. (2.1) along with Eqs. (2.4)-(2.7) yields the EOMs for the three angular momenta vectors⁶ [40],

$$\frac{d\mathbf{s}_1}{dt} = \frac{1}{c^2 r^3} \left\{ \delta_1 \mathbf{l} + \left[-\nu \mathbf{s}_2 + \frac{3\mu}{m_1} (\mathbf{n} \cdot \mathbf{s}_0) \mathbf{n} \right] \right\} \times \mathbf{s}_1, \quad (2.8a)$$

$$\frac{d\mathbf{s}_2}{dt} = \frac{1}{c^2 r^3} \left\{ \delta_2 \mathbf{l} + \left[-\nu \mathbf{s}_1 + \frac{3\mu}{m_2} (\mathbf{n} \cdot \mathbf{s}_0) \mathbf{n} \right] \right\} \times \mathbf{s}_2, \quad (2.8b)$$

$$\frac{d\mathbf{l}}{dt} = \frac{1}{c^2 r^3} \{ \mathbf{s}_{\text{eff}} \times \mathbf{l} + [-3(\mathbf{n} \cdot \mathbf{s}_0)(\mathbf{n} \times \mathbf{s}_0)] \}, \quad (2.8c)$$

where the 2PN terms are displayed in the square brackets. These equations reveal important features of the 2PN spin dynamics.

First we see that the timescale of variation of spins is

$$\frac{\|\mathbf{s}_1\|}{\|d\mathbf{s}_1/dt\|} \sim \frac{c^2 r^3}{l} \sim c^2 a^{5/2}, \quad (2.9)$$

where a is the reduced semi major axis. This timescale is 1PN order larger than the orbital timescale $\tau_{\text{orb}} \sim a^{3/2}$. Also, the first terms on the right-hand sides of Eq. (2.8) arise from the spin-orbit couplings, while the remaining terms originate from spin-spin interactions. A crucial distinction from the 1.5PN case is that l , the magnitude of the orbital angular momentum, is no longer conserved at 2PN order. This can be verified by computing

$$\frac{d(l^2)}{dt} = 2\mathbf{l} \cdot \frac{d\mathbf{l}}{dt} = -\frac{6}{c^2 r^3} (\mathbf{n} \cdot \mathbf{s}_0) (\mathbf{l} \cdot (\mathbf{n} \times \mathbf{s}_0)) \neq 0. \quad (2.10)$$

In contrast, the spin magnitudes $s_1 = \|\mathbf{s}_1\|$ and $s_2 = \|\mathbf{s}_2\|$ remain constant, as can be shown by taking $\mathbf{s}_a \cdot d\mathbf{s}_a/dt = 0$ from the cross-product structure of Eqs. (2.8a) and (2.8b).

Another important consequence of the 2PN spin-spin interactions is that the quantity $\mathbf{l} \cdot \mathbf{s}_{\text{eff}}$, which is conserved at 1.5PN order, now varies with time [39]. These features prevent a direct application of the method developed in Ref. [34]. However, as we will demonstrate in Sec. 3, orbit averaging restores an analogous mathematical structure, which then allows one to get an analytical solution, see also Ref. [21].

3. SPIN SECTOR SOLUTION

A. General characteristics of spin dynamics

Before presenting our solution, let us review some general characteristics of the spin sector solution. This will help us strategize the construction of our solution. This subsection aims at presenting the general behaviour of the different existing and to-be-presented solutions, while the necessary mathematical justifications of our statements is delayed to later subsections.

We start with Fig. 1, where we plot S_{1x} for a certain initial condition. The two numerical plots correspond to the EOMs obtained from the 1.5PN and 2PN Hamiltonians. The plots immediately reveal the two-timescale feature of the solutions. The left panel of the figure clearly shows that S_{1x} primarily changes at the slower spin precession timescale, which is 1PN order larger than the orbital timescale. On the other hand, the zoomed-in version in the right panel shows the sub-dominant oscillations occurring on a much shorter orbital timescale τ_{orb} .

The oscillations at these two timescales have already been successfully incorporated in an analytical solution at the 1.5PN level by Cho and Lee in Ref. [34]. While constructing this solution, or later in Sec. 3C our ‘‘hybrid solution’’, one must inject a lower order (Newtonian or 1PN) r solution into a differential equation governing the change of the cosine of the angle between \mathbf{S} and \mathbf{L} ⁷. As will be made clear in Sec. 3C, the PN accuracy of this injected r solution determines the PN accuracy of the slow and fast frequencies, and hence the dynamics associated with them. This is clearly borne out in the plots of Fig. 1, where the analytical solution of S_{1x} obtained by the injection of Newtonian

⁶ Note that the EOMs in Eqs. (2.8)-(2.10) of Ref. [40] have a typo. The sign associated with $(\hat{\mathbf{n}} \cdot \mathbf{S}_0) \hat{\mathbf{n}} \times \mathbf{S}_0$ in their Eq. (2.10) should be flipped to a minus. The same typo propagates to its Eq. (3.2c).

⁷ See Eq. (3.4) of Ref. [34] or our Eq. (3.43) for a precise definition.

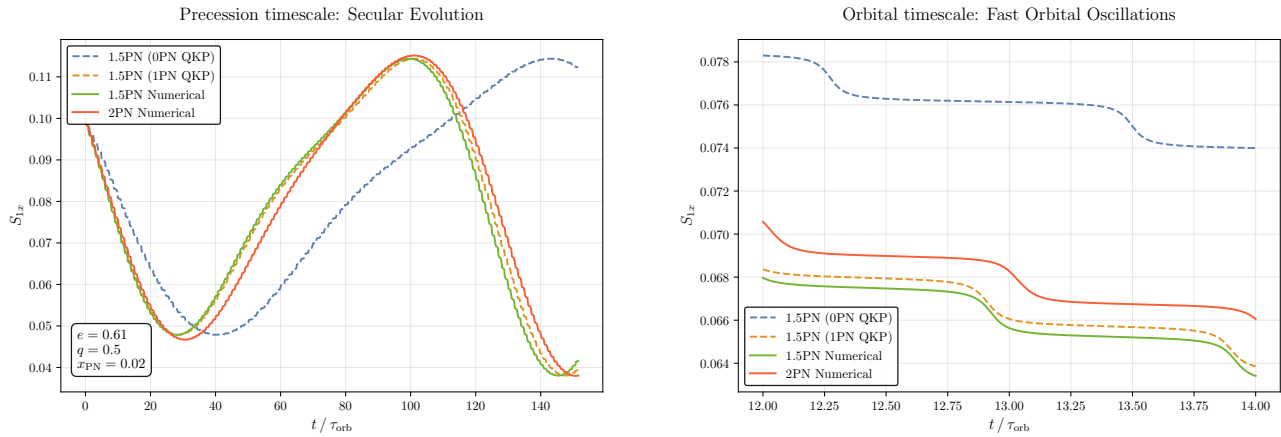


FIG. 1: Evolution of $\mathbf{S}_{1,x}$ for an eccentric BBH with $e = 0.61$, $q \equiv m_2/m_1 = 0.5$, and $x_{\text{PN}} = 2 \times 10^{-2}$. Initial angles: $\langle \mathbf{L}, \mathbf{S}_1 \rangle = 32^\circ$, $\langle \mathbf{L}, \mathbf{S}_2 \rangle = 82^\circ$, $\langle \mathbf{S}_1, \mathbf{S}_2 \rangle = 54^\circ$. We compare the evolution under four different evolution schemes: 1.5PN solution with Newtonian r injected (0PN QKP, blue dashed), the same analytical solution with 1PN r injected (1PN QKP, orange dashed), 1.5PN numerical solution (green), and 2PN numerical solution (red). *Left*: Evolution over one slow precession period. *Right*: Two-orbit zoomed-in view into the time interval $[12\tau_{\text{orb}}, 14\tau_{\text{orb}}]$, highlighting the fast orbital-timescale oscillations.

(resp. 1PN) r is plotted in blue (resp. orange). It is remarkable to note the improvement brought about by injecting the 1PN solution for r , over simply injecting the Newtonian r ⁸.

The left panel of Fig. 1 isolates the *slow-frequency* evolution over a full precession period. If a Newtonian orbital parametrization is used, the 1.5PN analytical solution suffers from a severe, continuously accumulating secular dephasing relative to the numerical results. Upgrading the underlying orbit to 1PN reduces this drift significantly, as the 1PN orbital dynamics feed directly into the precession and nutation frequencies [see Eqs. (I.1) and (I.2)]. However, a slight phase mismatch relative to the full 2PN numerical integration remains. This residual dephasing is expected, as the 1.5PN analytical model lacks the 2PN spin–spin interactions necessary to fully capture the higher-order shifts in the secular precession rate.

The right panel focuses on a two-orbit interval to highlight the *fast-frequency* oscillations. If a Newtonian orbital parametrization is used, the 1.5PN analytical solution exhibits a distinct orbital frequency mismatch, manifesting as a pronounced time shift during the periastron kicks. Upgrading the underlying orbit to 1PN reduces this fast-frequency dephasing substantially, bringing the analytical timing into close alignment with the 1.5PN numerical integration.

In the following sections, we construct our solution in two steps. First, we use an orbit-averaged approach (Sec. 3B) to incorporate the 2PN spin–spin contributions that improve the slow precessional envelope. Second, to recover the fast orbital oscillations while preserving this secular behavior, we introduce a hybrid solution (Sec. 3C) that blends the orbit-averaged dynamics with the leading-order oscillatory features.

B. Orbit averaged solution

1. Orbit averaged equations of motion

We now orbit-average Eq. (2.8) to obtain the secular spin dynamics. Following the discussion in Sec. 3A, we average the leading-order (LO) spin-orbit terms over the 1PN orbit, while the next-to-leading-order (NLO) spin-spin terms in the square brackets are averaged over a Newtonian orbit. At this point, let us mention that averaging the LO terms over the 1PN rather than the Newtonian orbit improves the accuracy of the slow precession frequency at the cost of introducing a beyond-2PN correction. As a consequence, certain segments of our solution contain terms that are formally more than 2PN accurate. Since our EOMs are only 2PN accurate, the beyond-2PN accuracy of our solution

⁸ Injection of the 1PN solution for r is an instance of the unphysical more-than-2PN accuracy that we mentioned at the end of Sec. 1B. This is so because moving from Newtonian to 1PN represents a jump in accuracy of 1PN, to reach 2.5PN, whereas our work aims to increase it by only half a unit (1.5PN to 2PN).

is not physical. The reason we still choose to retain these terms is that they give us useful insights for increasing the real physical PN accuracy if we were to start off with higher PN EOMs.⁹

The averages are computed by treating the angular momenta as constant over an orbital period. For the LO terms, we employ the 1PN quasi-Keplerian parametrization of Ref. [24],

$$r = a_r(1 - e_r \cos u), \quad (3.1)$$

$$n(t - t_0) = u - e_t \sin u, \quad (3.2)$$

where the reduced quasi-Keplerian orbital elements are defined as

$$a_r = -\frac{1}{2h} \left(1 - \frac{(\nu - 7)h}{2c^2} \right), \quad (3.3)$$

$$e_r^2 = 1 + 2hl^2 - \frac{2(6 - \nu)h}{c^2} - \frac{5(3 - \nu)h^2 l^2}{c^2}, \quad (3.4)$$

$$n = (-2h)^{3/2} \left(1 + \frac{(15 - \nu)h}{4c^2} \right), \quad (3.5)$$

$$e_t^2 = 1 + 2hl^2 + \frac{4(1 - \nu)h}{c^2} + \frac{(17 - 7\nu)h^2 l^2}{c^2}. \quad (3.6)$$

Additionally, we define $d_0 \equiv a\sqrt{1 - e^2}$, where a and e are the Newtonian limits of a_r and e_r .

The two orbit averages required to evaluate Eq. (2.8) are

$$\left\langle \frac{1}{r^3} \right\rangle = \frac{1}{d^3}, \quad (3.7a)$$

$$\left\langle \frac{n^i n^j}{r^3} \right\rangle = \frac{1}{2d_0^3} \left(\delta^{ij} - \frac{l^i l^j}{l^2} \right), \quad (3.7b)$$

where the 1PN d is given by

$$d \equiv a_r \sqrt{1 - e_\theta^2}, \quad e_\theta \equiv \frac{3e_r - e_t}{2}. \quad (3.8)$$

Consistently with our prescription, the first average is evaluated over the 1PN orbit, while the second, which multiplies the NLO spin-spin terms, is evaluated over the Newtonian orbit.

Substituting these results into Eq. (2.8) yields the orbit averaged equations of motion¹⁰

$$\left\langle \frac{d\mathbf{s}_1}{dt} \right\rangle = \frac{1}{c^2 d^3} \left\{ \delta_1 \mathbf{1} + \left[-\frac{3\mu}{2m_1} \lambda \mathbf{1} + \frac{\nu}{2} \mathbf{s}_2 \right] \right\} \times \mathbf{s}_1, \quad (3.9a)$$

$$\left\langle \frac{d\mathbf{s}_2}{dt} \right\rangle = \frac{1}{c^2 d^3} \left\{ \delta_2 \mathbf{1} + \left[-\frac{3\mu}{2m_2} \lambda \mathbf{1} + \frac{\nu}{2} \mathbf{s}_1 \right] \right\} \times \mathbf{s}_2, \quad (3.9b)$$

$$\left\langle \frac{d\mathbf{l}}{dt} \right\rangle = \frac{1}{c^2 d^3} \left\{ \mathbf{s}_{\text{eff}} + \left[-\frac{3}{2} \lambda \mathbf{s}_0 \right] \right\} \times \mathbf{l}. \quad (3.9c)$$

If we had calculated the average for a Newtonian orbit, we would have obtained the equations from Ref. [40], which take the same form but with d replaced by d_0 . Henceforth, for notational brevity, we drop the explicit orbit-average symbols $\langle \cdot \rangle$, with the understanding that all quantities represent orbit-averaged variables, up to Sec. 3C.

Eqs. (3.9) admit the conserved quantity

$$\lambda \equiv \frac{\mathbf{l} \cdot \mathbf{s}_0}{l^2}, \quad (3.10)$$

⁹ Orbit averaging over the 1PN orbit is another instance of the unphysical accuracy mentioned in Sec. 1B: moving from Newtonian to 1PN represents a jump in accuracy of 1PN, to reach 2.5PN, whereas our work aims to increase it by only half a unit (1.5PN to 2PN).

¹⁰ Strictly, the hybrid averaging procedure leads to a factor of $1/d_0^3$ for the NLO terms. However, replacing d_0 with d induces only 3PN-level changes, which we neglect.

first identified in Ref. [40]. This constant of motion arises strictly after orbit-averaging and plays a crucial role in the integrability of the dynamics. A key feature of these equations is their uniform cross-product structure:

$$\frac{d\mathbf{f}}{dt} = \boldsymbol{\Omega}_{\mathbf{f}} \times \mathbf{f}, \quad (3.11)$$

where $\mathbf{f} \in \{\mathbf{s}_1, \mathbf{s}_2, \mathbf{l}\}$ and $\boldsymbol{\Omega}_{\mathbf{f}}$ denotes the corresponding precession frequency vector. This structure implies that the magnitudes s_1 , s_2 , and l remain constant. Moreover, these equations take the same mathematical form as the 1.5PN spin-precession system solved analytically in Ref. [34], allowing those solution techniques to be directly extended to the present 2PN orbit averaged dynamics.

2. The solution of $\cos \kappa_1$

Here we work out the solution of Eqs. (3.9) in the style of Ref. [34] which differs in presentation from an equivalent solution presented in Ref. [21].

The angles between the three pairs of angular momenta satisfy the following relationships

$$\cos \gamma \equiv \frac{\mathbf{s}_1 \cdot \mathbf{s}_2}{s_1 s_2}, \quad (3.12a)$$

$$\cos \kappa_1 \equiv \frac{\mathbf{l} \cdot \mathbf{s}_1}{l s_1}, \quad (3.12b)$$

$$\cos \kappa_2 \equiv \frac{\mathbf{l} \cdot \mathbf{s}_2}{l s_2}, \quad (3.12c)$$

Using Eqs. (3.9), we can derive the time evolution of these angles. A key observation is that all three derivatives are proportional to the same quantity $\mathbf{l} \cdot (\mathbf{s}_1 \times \mathbf{s}_2)$

$$\frac{d \cos \gamma}{dt} = \frac{(\delta_1 - \delta_2)(1 - \lambda)}{c^2 d^3} \frac{1}{s_1 s_2} \mathbf{l} \cdot (\mathbf{s}_1 \times \mathbf{s}_2), \quad (3.13a)$$

$$\frac{d \cos \kappa_1}{dt} = \frac{(\delta_2 - \nu/2)(1 - \lambda)}{c^2 d^3} \frac{1}{l s_1} \mathbf{l} \cdot (\mathbf{s}_1 \times \mathbf{s}_2), \quad (3.13b)$$

$$\frac{d \cos \kappa_2}{dt} = -\frac{(\delta_1 - \nu/2)(1 - \lambda)}{c^2 d^3} \frac{1}{l s_2} \mathbf{l} \cdot (\mathbf{s}_1 \times \mathbf{s}_2). \quad (3.13c)$$

This proportionality allows us to construct two additional constants of motion by taking appropriate linear combinations. Following Cho and Lee [34], we define

$$\Sigma_1 = \cos \gamma + \frac{m_1 - m_2}{m_1} \frac{l}{s_2} \cos \kappa_1, \quad (3.14a)$$

$$\Sigma_2 = \cos \kappa_2 + \frac{m_2 s_1}{m_1 s_2} \cos \kappa_1. \quad (3.14b)$$

In the absence of gravitational-wave emission, the total angular momentum $\mathbf{J} = \mathbf{L} + \mathbf{S}_1 + \mathbf{S}_2$ is conserved. In the conservative, orbit-averaged dynamics, the magnitudes $\|\mathbf{L}\|$, $\|\mathbf{S}_1\|$, and $\|\mathbf{S}_2\|$ are also conserved. Together with the two additional constants of motion Σ_1 and Σ_2 introduced above, this yields eight constants for the nine components of \mathbf{L} , \mathbf{S}_1 , and \mathbf{S}_2 . As a result, the evolution of the full system is governed by a single independent dynamical degree of freedom. Following the reasoning of Cho and Lee [34], we choose this degree of freedom to be $\cos \kappa_1$, defined in Eq. (3.12b). The periodicity of this degree of freedom defines the nutation frequency of the spin subsystem; see Appendix I for a complete description of the four fundamental frequencies governing the 2PN dynamics. We now derive the 2PN orbit-averaged solution for $\cos \kappa_1$.

Using Eq. (3.14), we can express $\mathbf{l} \cdot (\mathbf{s}_1 \times \mathbf{s}_2)$ in terms of $\cos \kappa_1$ and constants of motion (see Appendix A). We get

$$\frac{\mathbf{l} \cdot (\mathbf{s}_1 \times \mathbf{s}_2)}{l s_1} = \pm \sqrt{A_3 x^3 + A_2 x^2 + A_1 x + A_0}, \quad (3.15)$$

where $x \equiv \cos \kappa_1$ and the coefficients are

$$A_3 = \frac{2(m_1 - m_2)m_2}{m_1^2} l s_1, \quad (3.16a)$$

$$A_2 = -\frac{1}{m_1^2} \left((m_1 - m_2)^2 l^2 + m_2^2 s_1^2 + m_1^2 s_2^2 + 2m_1 m_2 s_1 s_2 \Sigma_1 + 2m_1(m_1 - m_2) l s_2 \Sigma_2 \right), \quad (3.16b)$$

$$A_1 = \frac{2s_2}{m_1} \left((m_1 - m_2) l \Sigma_1 + (m_2 s_1 + m_1 s_2 \Sigma_1) \Sigma_2 \right), \quad (3.16c)$$

$$A_0 = (1 - \Sigma_1^2 - \Sigma_2^2) s_2^2. \quad (3.16d)$$

We define the roots of the cubic polynomial in Eq. (3.15) as $x_- \leq x_+ < x_3$ (derived in Appendix B). While Cho and Lee [34] proved the existence of real roots for x , we adopt this specific ordering to bound the physical motion of $\cos \kappa_1$ within $x_- \leq x \leq x_+$. Substituting Eq. (3.15) into Eq. (3.13b) yields a separable differential equation

$$\frac{dx}{\sqrt{A(x - x_-)(x - x_+)(x - x_3)}} = \frac{\pm dt}{c^2 d^3}, \quad (3.17)$$

where

$$A = \frac{9}{2} \frac{m_2(m_1 - m_2)}{(m_1 + m_2)^2} (1 - \lambda)^2 l s_1 > 0. \quad (3.18)$$

The key difference from the 1.5PN case treated by Ref. [34] is that the right-hand side of Eq. (3.17) is now $\pm dt/c^2 d^3$ rather than $\pm dt/c^2 r^3$, where we recall that $1/d^3$ is the orbit-average of $1/r^3$. This demonstrates that the fast oscillations are effectively averaged out. The left hand side of Eq. (3.17) can be integrated using elliptic integrals, which yields the quasi-Keplerian parametrization of $\cos \kappa_1$

$$\cos \kappa_1(t) = x_- + (x_+ - x_-) \operatorname{sn}^2(\Upsilon(t), \beta), \quad (3.19)$$

where $\operatorname{sn}(u, k)$ denotes the Jacobi elliptic sine function with argument u and modulus k , defined through its relation to the incomplete elliptic integral of the first kind

$$\operatorname{sn}(u, k) = \sin(\operatorname{am}(u, k)) = \sin \varphi, \quad \text{where } u = F(\varphi, k) = \int_0^\varphi \frac{d\theta}{\sqrt{1 - k^2 \sin^2 \theta}}. \quad (3.20)$$

Here $\operatorname{am}(u, k)$ is the Jacobi amplitude function, which gives the angle φ corresponding to the elliptic integral value u . The parameters appearing in Eq. (3.19) are

$$\Upsilon(t) = \frac{\sqrt{A(x_3 - x_-)}}{2} \left(\alpha + \frac{t}{c^2 d^3} \right), \quad (3.21a)$$

$$\beta = \sqrt{\frac{x_+ - x_-}{x_3 - x_-}}, \quad (3.21b)$$

$$\alpha = \pm \frac{2}{\sqrt{A(x_3 - x_-)}} F \left(\arcsin \sqrt{\frac{x(t_0) - x_-}{x_+ - x_-}}, \beta \right), \quad (3.21c)$$

with $F(\varphi, k)$ being the incomplete elliptic integral of the first kind as defined above. The sign in Eq. (3.21c) is chosen to match the initial condition: + if $d \cos \kappa_1 / dt > 0$ at initial time t_0 , and - otherwise.

The main distinction from the solution presented in Ref. [34] is that Υ varies linearly with time. As a result, the formulation in Eq. (3.21) not only neglects the fast oscillations appearing at 2PN order, but also fails to reproduce the 1.5PN oscillations obtained in Ref. [34]. Nevertheless, all the secular effects are correctly captured up to 2PN order. The time evolution of $\cos \kappa_2$ and $\cos \gamma$ follows directly from Eqs. (3.14) and (3.19). Finally, the remaining relative angles can also be expressed using the solution of $\cos \kappa_1$ and are given explicitly in Appendix C which uses Eq. (3.24).

This is a good time to reflect on what the above solution tell us. Υ of Eq. (3.21a) acts like the phase of the sn function. We see that $1/d^3$ is a prefactor multiplying the time t . Recall from our earlier discussion in Sec. 3B1 that we would have d_0 instead of d had we chosen to orbit-average over the Newtonian orbit. Since this prefactor determines the slow frequency of motion governing the evolution of $\cos \kappa_1$, we can conclude that the slow frequency is determined by the background orbit being averaged over (via d).

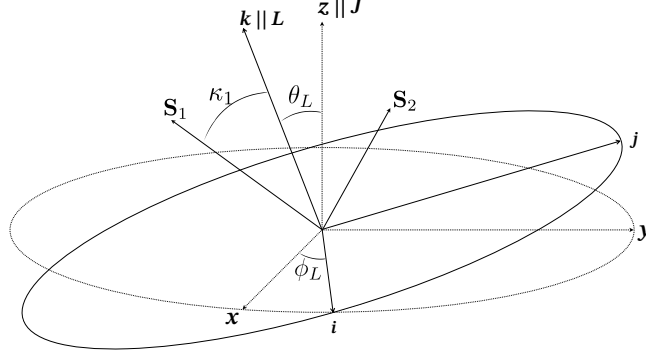


FIG. 2: The dashed frame represents the inertial frame (IF) $(\mathbf{x}, \mathbf{y}, \mathbf{z})$ centered around \mathbf{J} . The solid frame is the non-inertial frame (NIF) $(\mathbf{i}, \mathbf{j}, \mathbf{k})$ centered around \mathbf{L} .

From our above discussion and the one in Sec. 3A, we see that both the OA and unaveraged solutions for the angular momenta $(\mathbf{s}_1, \mathbf{s}_2, \mathbf{l})$ require a lower-PN-order underlying solution $\mathbf{r}(t)$ of the orbital dynamics, which is used to perform orbit averaging in the former case and “injection” of $r(t)$ in the latter. This orbital solution ends up affecting the slow frequency in both cases. In this sense, the choice of the orbit to average over (Newtonian or 1PN) in the case of OA solutions is similar, if not equivalent, to the choice of which r to inject while constructing the unaveraged solutions.

3. Solution for the orbit-averaged orbital angular momentum

Having determined the evolution of the angles between the angular momenta vectors, we now construct the explicit time dependence of \mathbf{L} in an inertial frame. We define two frames

- **Inertial Frame (IF):** an orthonormal basis $(\mathbf{x}, \mathbf{y}, \mathbf{z})$ with the z -axis aligned with the conserved total angular momentum \mathbf{J} .
- **Non-Inertial Frame (NIF):** an orthonormal basis $(\mathbf{i}, \mathbf{j}, \mathbf{k})$ obtained by rotating the IF such that the k -axis aligns with \mathbf{L} .

The transformation from the IF to the NIF is accomplished through two successive rotations, first by an angle ϕ_L around the z -axis, then by the angle θ_L around the x -axis, as is visualized in Fig. 2. The corresponding Euler rotation matrix is

$$\Lambda_{\text{IF} \rightarrow \text{NIF}} = \begin{pmatrix} \cos \phi_L & \sin \phi_L & 0 \\ -\sin \phi_L \cos \theta_L & \cos \phi_L \cos \theta_L & \sin \theta_L \\ \sin \phi_L \sin \theta_L & -\cos \phi_L \sin \theta_L & \cos \theta_L \end{pmatrix}. \quad (3.22)$$

Given that the magnitude of \mathbf{L} is conserved, its temporal evolution is entirely determined by the time evolution of the angles θ_L and ϕ_L . The angle θ_L represents the inclination of \mathbf{L} relative to \mathbf{J} and can be determined from

$$\cos \theta_L = \frac{\mathbf{l} \cdot \mathbf{j}}{l j} = \frac{l^2 + l s_1 \cos \kappa_1 + l s_2 \cos \kappa_2}{l j}. \quad (3.23)$$

Given the solutions for $\cos \kappa_1(t)$ and $\cos \kappa_2(t)$, Eq. (3.23) immediately yields $\theta_L(t)$.

To determine $\phi_L(t)$, we first need the expressions of the angular momenta vectors in the NIF

$$\mathbf{l} = l \begin{bmatrix} 0 \\ 0 \\ 1 \end{bmatrix}_{\text{NIF}}, \quad \mathbf{s}_1 = s_1 \begin{bmatrix} \sin \kappa_1 \cos \phi_{s1} \\ \sin \kappa_1 \sin \phi_{s1} \\ \cos \kappa_1 \end{bmatrix}_{\text{NIF}}, \quad \mathbf{s}_2 = s_2 \begin{bmatrix} \sin \kappa_2 \cos \phi_{s2} \\ \sin \kappa_2 \sin \phi_{s2} \\ \cos \kappa_2 \end{bmatrix}_{\text{NIF}}, \quad (3.24)$$

where ϕ_{s1} and ϕ_{s2} respectively denote the azimuthal angles of \mathbf{s}_1 and \mathbf{s}_2 in the NIF.

Since vector time derivatives become different geometrical objects depending on which frame is the time derivative being taken in, at this point, we establish that all vector time derivatives in this article are meant to be taken in the

inertial frame IF. Their components may be displayed in either of the two frames, IF or NIF. With that established, using Eq. (3.22), we first write the time derivative of \mathbf{l} in the IF and then transform the components to the NIF

$$\frac{d\mathbf{l}}{dt} = l \begin{pmatrix} \sin\theta_L \dot{\phi}_L \\ -\theta_L \\ 0 \end{pmatrix}_{\text{NIF}}. \quad (3.25)$$

We then equate this expression to Eq. (3.9c), after first evaluating the latter in the NIF using Eq. (3.24). By rearranging the first component, we obtain (see Appendix C)

$$\frac{d\phi_L}{dt} = \frac{1}{c^2 d^3} \left(\frac{\beta_{1L}}{\alpha_{1L} + \cos\kappa_1} - \frac{\beta_{2L}}{\alpha_{2L} + \cos\kappa_1} + \beta_{3L} \right), \quad (3.26)$$

where

$$\alpha_{1L} = \frac{m_1}{m_1 - m_2} \frac{j + l + s_2 \Sigma_2}{s_1}, \quad (3.27a)$$

$$\beta_{1L} = \frac{3m_1}{4(m_1^2 - m_2^2)} \frac{1}{s_1} (1 - \lambda) [m_1 j^2 + m_2 l^2 + (m_1 + m_2)jl - (m_1 - m_2)s_1(s_1 + s_2 \Sigma_1) + (m_2 l + m_1 j)s_2 \Sigma_2], \quad (3.27b)$$

$$\beta_{3L} = \frac{j\nu}{2}. \quad (3.27c)$$

The coefficients α_{2L} and β_{2L} are obtained from α_{1L} and β_{1L} by the substitution $j \rightarrow -j$.

Finally, Eq. (3.26) can be integrated using the incomplete elliptic integral of the third kind

$$\Pi(a, b, c) \equiv \int_0^b \frac{1}{\sqrt{1 - c^2 \sin^2 \theta}} \frac{d\theta}{1 - a \sin^2 \theta}. \quad (3.28)$$

The solution is

$$\phi_L(t) - \phi_L(t_0) = \frac{2}{\sqrt{A(x_3 - x_-)}} \left(\frac{\beta_{1L} \Pi\left(\frac{x_- - x_+}{\alpha_{1L} + x_-}, \text{am}(\Upsilon, \beta), \beta\right)}{\alpha_{1L} + x_-} - \frac{\beta_{2L} \Pi\left(\frac{x_- - x_+}{\alpha_{2L} + x_-}, \text{am}(\Upsilon, \beta), \beta\right)}{\alpha_{2L} + x_-} + \beta_{3L} \Upsilon \right). \quad (3.29)$$

The Eqs. (3.23) and (3.29), together with the conserved magnitude L , completely determine the time evolution of the averaged orbital angular momentum vector $\mathbf{L}(t)$ in the inertial frame.

4. Solution for the orbit-averaged spins angular momenta

The solutions for \mathbf{S}_1 and \mathbf{S}_2 follow an analogous procedure. For each spin, we construct a non-inertial frame by rotating the IF such that the k -axis aligns with the respective spin vector. The orientation of this frame relative to the IF is characterized by two angles $(\theta_{S_a}, \phi_{S_a})$ for $a \in \{1, 2\}$.

For \mathbf{S}_1 , the angle θ_{S_1} (inclination relative to \mathbf{J}) is given by

$$\cos\theta_{S_1} = \frac{\mathbf{s}_1 \cdot \mathbf{j}}{s_1 j} = \frac{s_1^2 + l s_1 \cos\kappa_1 + s_1 s_2 \cos\gamma}{s_1 j}, \quad (3.30)$$

which is immediately determined from the known evolution of $\cos\kappa_1$ and $\cos\gamma$.

The azimuthal angle ϕ_{S_1} satisfies

$$\frac{d\phi_{S_1}}{dt} = \frac{1}{c^2 d^3} \left(\frac{\beta_{1S_1}}{\alpha_{1S_1} + \cos\kappa_1} - \frac{\beta_{2S_1}}{\alpha_{2S_1} + \cos\kappa_1} + \beta_{3S_1} \right), \quad (3.31)$$

with coefficients

$$\alpha_{1S_1} = \frac{m_1}{m_2} \frac{1}{l} (-j + s_1 + s_2 \Sigma_1), \quad (3.32a)$$

$$\beta_{1S_1} = \frac{m_1}{4m_2} \frac{1}{l} \left[\left(2\delta_2 - \frac{3\mu}{m_2} \lambda \right) j^2 - \left(2\delta_1 - \frac{3\mu}{m_1} \lambda \right) l^2 - \nu (s_1^2 + s_2^2 + 2s_1 s_2 \Sigma_1 + 2l s_2 \Sigma_2) - 3 \left(\frac{2m_1 - m_2}{m_1 + m_2} \right) (1 - \lambda) j s_1 \right. \\ \left. + 3 \frac{(m_1^2 - m_2^2)}{(m_1 + m_2)^2} (1 - \lambda) (s_1^2 + s_1 s_2 \Sigma_1) - 3 \left(\frac{1 - \lambda}{m_1 + m_2} \right) (m_1 j \Sigma_1 + m_2 l \Sigma_2) s_2 \right], \quad (3.32b)$$

$$\beta_{3s_1} = \left(\delta_2 - \frac{3\mu}{2m_2} \lambda \right) j. \quad (3.32c)$$

The coefficients α_{2S_1} and β_{2S_1} are obtained from α_{1S_1} and β_{1S_1} by the substitution $j \rightarrow -j$.

Integrating Eq. (3.31) yields

$$\phi_{S_1}(t) - \phi_{S_1}(t_0) = \frac{2}{\sqrt{A(x_3 - x_-)}} \left(\frac{\beta_{1S_1} \Pi \left(\frac{x_- - x_+}{\alpha_{1S_1} + x_-}, \text{am}(\Upsilon, \beta), \beta \right)}{\alpha_{1S_1} + x_-} - \frac{\beta_{2S_1} \Pi \left(\frac{x_- - x_+}{\alpha_{2S_1} + x_-}, \text{am}(\Upsilon, \beta), \beta \right)}{\alpha_{2S_1} + x_-} + \beta_{3S_1} \Upsilon \right). \quad (3.33)$$

Finally, \mathbf{S}_2 can be obtained either by an analogous calculation or by using conservation of total angular momentum

$$\mathbf{S}_2 = \mathbf{J} - \mathbf{L} - \mathbf{S}_1. \quad (3.34)$$

This completes the solution for the orbit-averaged dynamics of the angular momenta. All vectors are expressed in terms of elliptic and elementary functions of time, with coefficients determined by the conserved quantities of the system.

C. Beyond orbit averaging: the hybrid solution for the spin sector

Let us summarize the situation so far. The solution presented in Secs. 3B2-3B4 is 2PN accurate for long timescale oscillations, but lacks the short timescale oscillations due to orbit-averaging. Insofar as the short timescale oscillations are concerned, they have been faithfully captured by the solution provided in Refs. [35] (based on Ref. [34]). But these solutions are only 1.5PN accurate. As discussed in Secs. 3A-3B2, the missing 2PN effects lead to inaccurate slow and fast frequencies. The purpose of this subsection is to construct a solution that is fully 1.5PN accurate for the fast oscillations, but additionally 2PN accurate in the slow dynamics. This model can be considered as a hybridization of the full 1.5PN accurate solution of Ref. [35] and the 2PN OA solution of Ref. [21] (re-presented above in Secs. 3B2-3B4), we call this solution the ‘‘hybrid model’’. We will see that the hybrid solution provides the most faithful approximation to the exact, numerical 2PN dynamics, at both timescales.

Consider the phase space variable \mathbf{s}_1 . Its evolution can be considered at various different levels of approximations: (i) full 2PN dynamics (to be labeled with ‘‘(2)’’) defined by numerical solution of the full 2PN EOMs Eqs. (2.8), (ii) the 1.5PN solution of Refs. [34, 35], to be labeled with ‘‘(1.5)’’ (iii) the 2PN OA dynamics, to be labeled with ‘‘(2, A)’’ (iv) the to-be-introduced hybrid model to be labeled with ‘‘(2, H)’’.

The EOMs for \mathbf{s}_1 under the evolution systems (2), (1.5) and (2, A), as defined above take the general form of a cross product

$$\frac{d\mathbf{s}_1^{(\cdot)}}{dt} = \boldsymbol{\Omega}^{(\cdot)} \times \mathbf{s}_1^{(\cdot)}, \quad (3.35)$$

where $\boldsymbol{\Omega}^{(\cdot)}$ denotes the precessional angular velocity and $\mathbf{s}_1^{(\cdot)}$ the corresponding spin solution for the model (\cdot) under consideration.

With the following definitions (where ‘‘SO’’ and ‘‘SS’’ stand for ‘‘spin-orbit’’ and ‘‘spin-spin’’), computed in Eqs. (2.8a) and (3.9),

$$\boldsymbol{\Omega}_{\text{SO}} = \frac{\delta_1}{c^2 r^3} \mathbf{1}, \quad \boldsymbol{\Omega}_{\text{SS}} = \frac{1}{c^2 r^3} \left(-\nu \mathbf{s}_2 + \frac{3\mu}{m_1} (\mathbf{n} \cdot \mathbf{s}_0) \mathbf{n} \right), \quad (3.36)$$

$$\bar{\boldsymbol{\Omega}}_{\text{SO}} \equiv \frac{\delta_1}{c^2 d^3} \mathbf{1}, \quad \bar{\boldsymbol{\Omega}}_{\text{SS}} \equiv \frac{1}{c^2 d^3} \left(\frac{\nu}{2} \mathbf{s}_2 - \frac{3\mu}{2m_1} \lambda \mathbf{1} \right), \quad (3.37)$$

the EOMs for \mathbf{s}_1 and the corresponding $\boldsymbol{\Omega}^{(\cdot)}$ for the leading 1.5PN spin dynamics is given by

$$\frac{d\mathbf{s}_1^{(1.5)}}{dt} = \boldsymbol{\Omega}^{(1.5)} \times \mathbf{s}_1^{(1.5)}, \quad \boldsymbol{\Omega}^{(1.5)} = \boldsymbol{\Omega}_{\text{SO}}. \quad (3.38)$$

At NLO, the full 2PN evolution incorporates both SO and SS couplings and reads

$$\frac{d\mathbf{s}_1^{(2)}}{dt} = \boldsymbol{\Omega}^{(2)} \times \mathbf{s}_1^{(2)}, \quad \boldsymbol{\Omega}^{(2)} = \boldsymbol{\Omega}_{\text{SO}} + \boldsymbol{\Omega}_{\text{SS}}. \quad (3.39)$$

The orbit-averaged 2PN spin evolution is given by

$$\frac{d\mathbf{s}_1^{(2,A)}}{dt} = \boldsymbol{\Omega}^{(2,A)} \times \mathbf{s}_1^{(2,A)}, \quad \boldsymbol{\Omega}^{(2,A)} = \bar{\boldsymbol{\Omega}}_{\text{SO}} + \bar{\boldsymbol{\Omega}}_{\text{SS}}. \quad (3.40)$$

Finally, we introduce our 2PN hybrid model defined by

$$\boldsymbol{\Omega}^{(2,H)} \equiv \frac{1}{c^2 r^3} \left(\delta_1 \mathbf{l} + \frac{\nu}{2} \mathbf{s}_2 - \frac{3\mu}{2m_1} \lambda \mathbf{l} \right) = \boldsymbol{\Omega}_{\text{SO}} + \frac{d^3}{r^3} \bar{\boldsymbol{\Omega}}_{\text{SS}}. \quad (3.41)$$

The above equation makes it apparent that this hybrid model is a 2PN perturbation of the 1.5PN dynamics. Hence the dynamics at both the slow and fast timescales are captured by this system at 1.5PN order.

Now let us come to 2PN order. It is easy to see from the above equations that if we were to OA the hybrid (2, H) model over the 1PN orbit (not Newtonian) then it will result in the 2PN OA (2, A) model. It is so because all that needs to be done to effect the orbit-averaging is to replace r with d in Eq. (3.41). Now recall from the discussion at the end of Sec. 3B2 that for OA solutions, the equivalent of orbit-averaging over a higher PN order orbit is to inject a higher PN order r solution in the evolution equation for $\cos \kappa_1$ (cosine of the angle between \mathbf{s}_1 and \mathbf{l}), since both these measures end up making the slow frequency more accurate. Of course, all this works because the (2, H) model shares the main mathematical characteristics with the (1.5) and (2, A) models ($\cos \kappa_1$ oscillating between the roots of a certain cubic polynomial, etc).

With all that established, what now remains to be done is to find the solution for the (2, H) model while remembering to inject 1PN r solution when solving the differential equation for $x = \cos \kappa_1$. Such a solution will capture the full 1.5PN dynamics of the three angular momenta, but only the slow timescale dynamics at 2PN. For completion, we write the hybrid EOMs for the angular momenta. To do so, d^3 is replaced by the instantaneous orbital separation r^3 in the denominators of the precession equations Eq. (2.8).

$$\frac{d\mathbf{s}_1}{dt} = \frac{1}{c^2 r^3} \left\{ \delta_1 \mathbf{l} + \left[-\frac{3\mu}{2m_1} \lambda \mathbf{l} + \frac{\nu}{2} \mathbf{s}_2 \right] \right\} \times \mathbf{s}_1, \quad (3.42a)$$

$$\frac{d\mathbf{s}_2}{dt} = \frac{1}{c^2 r^3} \left\{ \delta_2 \mathbf{l} + \left[-\frac{3\mu}{2m_2} \lambda \mathbf{l} + \frac{\nu}{2} \mathbf{s}_1 \right] \right\} \times \mathbf{s}_2, \quad (3.42b)$$

$$\frac{d\mathbf{l}}{dt} = \frac{1}{c^2 r^3} \left\{ \mathbf{s}_{\text{eff}} + \left[-\frac{3}{2} \lambda \mathbf{s}_0 \right] \right\} \times \mathbf{l}. \quad (3.42c)$$

Note that Eqs. (3.42) are very similar to two sets of evolution equations: the 1.5PN unaveraged EOMs (2.6) of Ref. [34], and the 2PN averaged EOMs (3.9). The former set features time varying r , unlike the latter set which features a constant d . Due to this, the method of finding the solution of Eqs. (3.42) is also very similar to that for EOMs (2.6) of Ref. [34], or Eqs. (3.9). We therefore will provide the final solution of Eqs. (3.42) rather than detailed derivation.

Before proceeding, we note that due to the presence of r^3 in Eqs. (3.42) (instead of d^3), we obtain, in place of Eq. (3.17), the following expression (like Eq. (3.4) of Ref. [34])

$$\frac{dx}{\sqrt{A(x-x_-)(x-x_+)(x-x_3)}} = \frac{\pm dt}{c^2 r^3} \quad (3.43)$$

At this point, we need to inject a lower order background r solution. The PN accuracy of this injected r influences the accuracy of both fast and slow frequencies, as we will see below. As already planned, we will inject the 1PN r of

Eqs. (3.1)-(3.6) into the above equation, rather than the Newtonian one (Newtonian r was injected in Ref. [34])¹¹. The quantities l , λ , Σ_1 , Σ_2 , the cubic polynomial, and its roots x_k remain constants of motion in the hybrid solution, preserving both the same expressions and numerical values as those obtained in the orbit-averaged case, which makes the solution feasible. During the course of derivation, we re-encounter the Eqs. (3.17), (3.26), and (3.31), except that d , in these equations, is replaced by r .

The final hybrid solution of Eqs. (3.42) is given by

$$\cos \kappa_1^{(2,H)}(t) = x_- + (x_+ - x_-) \operatorname{sn}^2(\Upsilon^{(2,H)}(t), \beta), \quad (3.44a)$$

$$\Upsilon^{(2,H)}(u) = \frac{\sqrt{A(x_3 - x_-)}}{2} \left[\alpha + \frac{1}{2c^2 n a_r^3} \left(\frac{(2 + e_r^2 - 3e_r e_t) v_r}{(1 - e_r^2)^{5/2}} + \frac{(e_r - e_t) \sin u}{(1 - e_r^2)(1 - e_r \cos u)^2} + \frac{(3e_r - e_t - 2e_r^2 e_t) \sin u}{(1 - e_r^2)^2(1 - e_r \cos u)} \right) \right], \quad (3.44b)$$

$$v_r = u + 2 \arctan \left(\frac{\beta_r \sin u}{1 - \beta_r \cos u} \right), \quad (3.44c)$$

$$\beta_r = \frac{e_r}{1 + \sqrt{1 - e_r^2}}, \quad (3.44d)$$

where the parameters A , α , β and the roots x_- , x_+ and x_3 are identical to those defined in Eqs. (3.18), (3.21), and (3.16) for the orbit-averaged case. The rest of the solution is given by Eqs. (3.23), (3.29), (3.30) and (3.33) but with the replacement $\Upsilon \rightarrow \Upsilon^{2,H}$. The evolution of u above is governed by the 1PN QKP solution of Eqs. (3.1) and (3.2).

One can clearly see that, whereas the orbit-averaged argument $\Upsilon^{(2,A)}$, which is Υ of Eq. (3.21a) grows linearly in time as $t/(c^2 d^3)$, the hybrid counterpart $\Upsilon^{(2,H)}$ contains additional oscillatory terms depending on the eccentric anomaly, which restore the fast orbital-timescale oscillations of the 1.5PN dynamics while preserving the correct secular behavior on the precession timescale.

What about the emergence of slow and fast frequencies? The argument $\Upsilon^{(2,H)}$ of the Jacobi sn function acts like a phase. The tiny, fast oscillations in this phase are brought about by v_r and functions of u in Eq. (3.44b) with the frequency of 1PN n ; this is due to Eqs. (3.44c) and (3.2). The slow frequency emerges due to the c^2 factor in the denominator, and hence is 1PN order smaller than the fast frequency. One final point to note is that both the slow and fast frequencies depend on the 1PN QKP parameters (e_r , e_t , a_r , n etc.) present in Eq. (3.44b). Hence the PN order of the injected r is essential to determine the accuracy of the two frequencies.

To assess the accuracy of the hybrid model relative to the other approximations, we derive in Appendix D analytical error bounds by comparing each approximate spin evolution to the full 2PN dynamics over times $t \lesssim \mathcal{O}(\tau_{\text{prec}}^{3/2})$

$$\|\mathbf{s}_1^{(1,5)}(t) - \mathbf{s}_1^{(2)}(t)\| \leq \mathcal{O}(t c^{-4}), \quad (3.45a)$$

$$\|\mathbf{s}_1^{(2,A)}(t) - \mathbf{s}_1^{(2)}(t)\| \leq \mathcal{O}(c^{-3}), \quad (3.45b)$$

$$\|\mathbf{s}_1^{(2,H)}(t) - \mathbf{s}_1^{(2)}(t)\| \leq \mathcal{O}(c^{-4}). \quad (3.45c)$$

These bounds reveal a clear hierarchy of accuracy whose significance depends on the timescale considered. On orbital timescales, $t \sim \tau_{\text{orb}} = \mathcal{O}(1)$, the 1.5PN and hybrid models achieve errors of $\mathcal{O}(c^{-4})$, accurately capturing the leading-order fast orbital oscillations. The orbit-averaged model exhibits a larger error, $\mathcal{O}(c^{-3})$, as it smooths out these oscillations. On precession timescales, $t \sim \tau_{\text{prec}} = \mathcal{O}(c^2)$, the 1.5PN error grows linearly to $\mathcal{O}(c^{-2})$ due to the missing secular spin-spin contributions, whereas both the averaged and hybrid models remain bounded at $\mathcal{O}(c^{-3})$ and $\mathcal{O}(c^{-4})$, respectively. The hybrid approach therefore combines the strengths of both descriptions, preserving the leading-order orbital oscillations of the 1.5PN model while correctly capturing the secular evolution, and is the most accurate approximation across all timescales.

Figure 3 provides a visual confirmation of these bounds¹². At short times ($t \sim \tau_{\text{orb}}$), orbital oscillations dominate and are faithfully reproduced by the 1.5PN and hybrid models, while secular deviations remain negligible. At intermediate times ($t \sim \mathcal{O}(c) \sim 20 \tau_{\text{orb}}$), secular spin-spin effects become significant: the orbit-averaged model begins to track the slow drift effectively, and its error becomes comparable to that of the 1.5PN model, as seen where the blue and green curves cross in the fourth column. As t approaches τ_{prec} , secular effects dominate; the averaged and hybrid models

¹¹This is yet another instance of the unphysical more-than-2PN accuracy that we mentioned at the end of Sec. 1B; see Footnote 8.

¹²To plot the 1.5PN solution, we used the 1PN QKP.

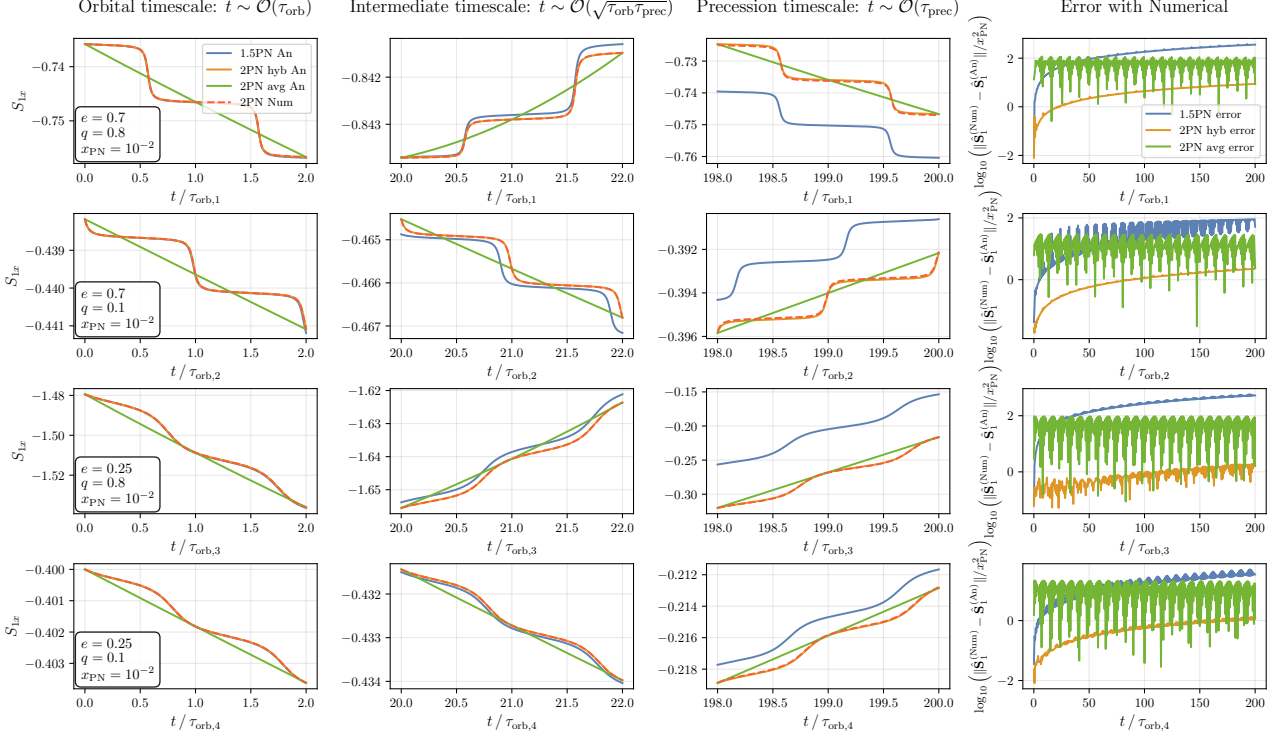


FIG. 3: Comparison of the spin vector \mathbf{S}_1 across approximate models against the full 2PN dynamics obtained by numerical integration (red). The 1.5PN solution (1.5) (blue), the hybrid model (2, H) (orange), and the orbit-averaged 2PN solution (2, A) (green) are shown. The hybrid model accurately recovers the leading-order fast orbital oscillations of the 2PN evolution while preserving the correct secular behavior; the orbit-averaged model reproduces only the secular evolution; and the 1.5PN model captures the oscillations but misses the secular spin-spin effects. Results are shown for four systems with different mass ratios ($q = m_2/m_1$) and eccentricities, all sharing the random same spin orientations: $\kappa_1 = 68^\circ$, $\kappa_2 = 10^\circ$, $\gamma = 73^\circ$. The first three columns display the x -component of \mathbf{S}_1 over increasing timescales, from orbital periods to precession times, while the fourth column shows the difference between each approximate solution and the numerical 2PN result. The vertical axis of the fourth column is normalized by $x_{\text{PN}} \sim 10^{-2}$: a value of $y = 0$ corresponds to a 2PN-level error ($\mathcal{O}(c^{-4})$), while $y = 2$ indicates the error has grown to 1PN order ($\mathcal{O}(c^{-2})$).

remain the most accurate, with the hybrid model uniquely capturing both the secular trend and the leading orbital oscillations. Quantitatively, the orbit-averaged difference (green) stays nearly constant around $y \sim 1$, the hybrid (orange) grows slowly and remains mostly below $y = 0$, while the 1.5PN model (blue) rises steadily from $y \lesssim 0$ to $y \gtrsim 2$. These trends confirm the analytical error bounds in Eq. (3.45) and demonstrate that the hybrid model effectively combines the strengths of the 1.5PN and orbit-averaged 2PN approaches.

4. THE QUASI-KEPLERIAN SOLUTION FOR THE ORBITAL DYNAMICS

We now turn to the orbital dynamics and derive a quasi-Keplerian parametric solution for eccentric orbits of the 2PN spinning system governed by the Hamiltonian (2.1). We first obtain the EOMs for the radial and azimuthal variables r and ϕ (azimuthal angle of \mathbf{r} in the NIF). Then we construct a solution using an ansatz-based approach analogous to that of Ref. [42]. When deriving the two EOMs, the angular momentum variables are taken to satisfy the 2PN full precession equations (2.8), rather than the hybrid description (3.42). In this section, the hybrid description is used only in Eq. (4.22), and solely to account for the precession of the non-inertial frame with respect to the inertial one.

A. Radial equation of motion

To start, we derive the equation of motion for the radial coordinate r by computing its Poisson bracket with the Hamiltonian (2.1). It yields

$$\begin{aligned} \left(\frac{dr}{dt}\right)^2 = & p_r^2 - \frac{1}{c^2} \left[(1-3\nu) p_r^4 + \left(\frac{1}{r}(6+4\nu) + \frac{l^2}{r}(1-3\nu) \right) p_r^2 \right] + \frac{1}{c^4} \left[\left(\frac{1}{r}(8-27\nu-14\nu^2) + \frac{l^2}{2r^2}(4-21\nu+24\nu^2) \right) p_r^4 \right. \\ & \left. + \frac{1}{4}(4-21\nu+24\nu^2) p_r^6 + \left(\frac{1}{r^2}(19+34\nu+4\nu^2) + \frac{l^2}{r^3}(8-27\nu-10\nu^2) + \frac{l^4}{4r^4}(4-21\nu+24\nu^2) \right) p_r^2 \right], \end{aligned} \quad (4.1)$$

where p_r is the canonical momentum conjugate to the radial separation r , such that

$$p_r^2 = (\mathbf{n} \cdot \mathbf{p})^2 = \mathbf{p}^2 - l^2/r^2. \quad (4.2)$$

We recall that in Eqs. (4.1) and Eq. (4.2), the norm of \mathbf{l} is no longer constant, as shown in Eq. (2.10). To express Eq. (4.1) solely in terms of r , h , l , and the spin variables, we need to eliminate p_r^2 . It is achieved by perturbatively inverting the Hamiltonian (2.1) to obtain p_r^2 as a PN expansion in powers of $1/c^2$. Keeping all the terms up to 2PN order, we find

$$p_r^2 = \tilde{A} + \frac{2\tilde{B}}{r} + \frac{\tilde{C}}{r^2} + \frac{\tilde{D}_1}{r^3} + \frac{\tilde{D}_2}{r^4} + \frac{\tilde{D}_3}{r^5} + \mathcal{O}\left(\frac{1}{c^5}\right), \quad (4.3)$$

where the coefficients \tilde{A} , \tilde{B} , \tilde{C} , $\tilde{D}_{1,2,3}$ are functions of h , l , and the spins, given in Eq. (E.1) of App. E. Finally, substituting Eq. (4.3) into Eq. (4.1) and collecting terms, we obtain the radial equation of motion in polynomial form

$$\left(\frac{dr}{dt}\right)^2 = A + \frac{2B}{r} + \frac{C}{r^2} + \frac{D_{1o} + D_{1s}}{r^3} + \frac{D_2}{r^4} + \frac{D_3}{r^5} + \mathcal{O}\left(\frac{1}{c^5}\right). \quad (4.4)$$

To compactly express the spin-spin contributions, we introduce a new mass-weighted spin vector

$$\mathcal{S} \equiv \frac{m_2}{m} \mathbf{s}_1 + \frac{m_1}{m} \mathbf{s}_2. \quad (4.5)$$

In terms of this variable, the radial coefficients take the following form:

$$A = 2h + \frac{1}{c^2} 3(-1 + 3\nu) h^2 + \frac{1}{c^4} (4 - 19\nu + 16\nu^2) h^3, \quad (4.6a)$$

$$B = 1 + \frac{1}{c^2} (-6 + 7\nu) h + \frac{1}{c^4} 3(3 - 16\nu + 7\nu^2) h^2, \quad (4.6b)$$

$$C = -l^2 + \frac{1}{c^2} [5(\nu - 2) + 2(1 - 3\nu) h l^2] + \frac{1}{c^4} [(37 - 122\nu + 36\nu^2) h - 3(1 - 5\nu + 5\nu^2) h^2 l^2], \quad (4.6c)$$

$$D_{1o} = \frac{1}{c^2} (8 - 3\nu) l^2 + \frac{1}{c^4} \left[\frac{53}{2} - \frac{83\nu}{2} + 10\nu^2 - (16 - 73\nu + 19\nu^2) h l^2 \right], \quad (4.6d)$$

$$D_{1s} = -\frac{1}{c^2} [2\mathbf{l} \cdot \mathbf{s}_{\text{eff}} - \mathcal{S}^2 + 3(\mathbf{n} \cdot \mathcal{S})^2], \quad (4.6e)$$

$$D_2 = -\frac{1}{c^4} 3(11 - 11\nu + 2\nu^2) l^2, \quad (4.6f)$$

$$D_3 = -\frac{1}{c^4} \frac{\nu(4 + \nu)}{4} l^4. \quad (4.6g)$$

When compared to the non-spinning or spin-orbit case, the main technical challenge in constructing a 2PN quasi-Keplerian parametrization for spinning binaries is that some coefficients in Eqs. (4.6) vary on orbital timescales. To determine which coefficients are time-dependent, we employ the two 2PN conserved quantities, denoted with a tilde,

derived in Ref. [39]. They are respectively deformed versions of $\mathbf{l} \cdot \mathbf{s}_{\text{eff}}$ and l^2 as,

$$\widetilde{\mathbf{l} \cdot \mathbf{s}_{\text{eff}}} = \mathbf{l} \cdot \mathbf{s}_{\text{eff}} + \frac{\nu}{2}(\mathbf{s}_1 \cdot \mathbf{s}_2) + \mathcal{O}(c^{-4}), \quad (4.7a)$$

$$\widetilde{l^2} = l^2 + \frac{1}{c^2} \left[2\nu(\mathbf{s}_1 \cdot \mathbf{s}_2)h + \frac{2}{r}(\mathbf{n} \cdot \boldsymbol{\mathcal{S}})^2 - (\mathbf{p} \cdot \boldsymbol{\mathcal{S}})^2 \right]. \quad (4.7b)$$

These conserved quantities reveal two key features of the dynamics. First, since $\widetilde{\mathbf{l} \cdot \mathbf{s}_{\text{eff}}}$ is a constant of motion and differs from $\mathbf{l} \cdot \mathbf{s}_{\text{eff}}$ only by the term $\frac{\nu}{2}(\mathbf{s}_1 \cdot \mathbf{s}_2)$ which evolves on the slow precession timescale, $\mathbf{l} \cdot \mathbf{s}_{\text{eff}}$ can be treated as effectively constant over an orbital period. The same argument applies to $\boldsymbol{\mathcal{S}}^2$ in Eq. (4.6). Second, Eq. (4.7b) reveals that $\widetilde{l^2}$ has oscillatory terms (featuring \mathbf{n} , \mathbf{p} and r) at relative 2PN order. These oscillatory terms oscillate at the orbital frequency.

We now examine the time dependence of each coefficient in Eqs. (4.6). The coefficients A and B depend only on the conserved Hamiltonian h and are therefore constant. The coefficients D_2 and D_3 depend on l^2 , but this dependence first appears at 2PN order. Since l^2 itself possesses 2PN oscillations, these oscillations contribute to D_2 and D_3 only at orders beyond 2PN, which we neglect. Thus A , B , D_2 , and D_3 are all effectively constant and retain the same functional forms as in the 2PN non-spinning case of Ref. [30]. In contrast, the coefficient C contains l^2 at Newtonian order. The 2PN oscillations of l^2 therefore cannot be neglected and induce a time dependence in C through the orbital-frequency terms in Eq. (4.7b). Similarly, $D_1 \equiv D_{1o} + D_{1s}$ is time-dependent because it depends explicitly on $(\mathbf{n} \cdot \boldsymbol{\mathcal{S}})^2$ in Eq. (4.6e), which oscillates with the orbital phase ϕ .

To rewrite the time-dependent dot products $(\mathbf{n} \cdot \boldsymbol{\mathcal{S}})$ and $(\mathbf{p} \cdot \boldsymbol{\mathcal{S}})$ appearing in C and D_1 , we work in the NIF where the orbital angular momentum \mathbf{L} is aligned with the k -axis. The orbital motion is confined to the ij -plane (see Fig. 2). At Newtonian order, the unit orbital separation and momentum vectors are given by

$$\mathbf{n} = \{\cos \phi, \sin \phi, 0\}, \quad (4.8a)$$

$$\mathbf{p} = \frac{1}{l} \{-\sin \phi, e + \cos \phi, 0\}. \quad (4.8b)$$

Next, we project the spin vectors onto the orbital plane, denoting them as $\mathbf{s}_{ap} \equiv \mathbf{s}_a - (\mathbf{s}_a \cdot \mathbf{k})\mathbf{k}$ with magnitude $s_{ap} = s_a \sin \kappa_a$. Here “ p ” signifies projection onto the orbital plane. Decomposing $\boldsymbol{\mathcal{S}}$ into its in-plane and orthogonal components ($\boldsymbol{\mathcal{S}} \equiv \boldsymbol{\mathcal{S}}_p + \boldsymbol{\mathcal{S}}_z$), we find

$$\boldsymbol{\mathcal{S}}_p = \frac{m_2}{m} \mathbf{s}_{1p} + \frac{m_1}{m} \mathbf{s}_{2p} \quad \text{and} \quad \boldsymbol{\mathcal{S}}_z = \left(\frac{m_2}{m} s_1 \cos \kappa_1 + \frac{m_1}{m} s_2 \cos \kappa_2 \right) \frac{\mathbf{l}}{l}. \quad (4.9)$$

The magnitude s_p and phase ϕ_s (measured from \mathbf{i} in the NIF) of $\boldsymbol{\mathcal{S}}_p$ are explicitly given by

$$s_p^2 = \frac{m_2^2}{m^2} s_{1p}^2 + \frac{m_1^2}{m^2} s_{2p}^2 + 2\nu s_{1p} s_{2p} \cos(\phi_{s1} - \phi_{s2}), \quad (4.10a)$$

$$\phi_s = \arctan \left(\frac{m_2 s_{1p} \sin \phi_{s1} + m_1 s_{2p} \sin \phi_{s2}}{m_2 s_{1p} \cos \phi_{s1} + m_1 s_{2p} \cos \phi_{s2}} \right). \quad (4.10b)$$

With these definitions, the oscillatory terms in Eq. (4.7) simplify to trigonometric functions of the phase difference $(\phi - \phi_s)$:

$$(\mathbf{n} \cdot \boldsymbol{\mathcal{S}})^2 = s_p^2 \cos^2(\phi - \phi_s), \quad (4.11a)$$

$$(\mathbf{p} \cdot \boldsymbol{\mathcal{S}})^2 = \frac{s_p^2}{l^2} (e \sin \phi_s - \sin(\phi - \phi_s))^2. \quad (4.11b)$$

Substituting Eqs. (4.11) into Eq. (4.7), the 2PN constant $\widetilde{l^2}$ can be rewritten as

$$\widetilde{l^2} = l^2 + \frac{1}{2c^2} \frac{s_p^2}{l^2} \left[(3e \cos(\phi - 2\phi_s) + 3 \cos(2\phi - 2\phi_s) + e \cos(3\phi - 2\phi_s)) + \left(1 - e^2 + 4\nu \frac{h l^2}{s_p^2} (\mathbf{s}_1 \cdot \mathbf{s}_2) + e^2 \cos 2\phi_s \right) \right]. \quad (4.12)$$

Since \tilde{l}^2 is a 2PN constant quantity, we can evaluate it at $\phi = 0$ and a general ϕ , and set these two evaluations equal to each other to express l^2 in terms of $l_0^2 \equiv l^2(\phi = 0)$:

$$l^2 = l_0^2 - \frac{1}{2c^2} \frac{s_p^2}{\tilde{l}^2} [(3e \cos(\phi - 2\phi_s) + 3 \cos(2\phi - 2\phi_s) + e \cos(3\phi - 2\phi_s)) - (3 + 4e) \cos 2\phi_s]. \quad (4.13)$$

From this equation, also present in [41], we observe that $l^2(\phi = 2\pi) = l_0^2$, indicating that the magnitude of the orbital angular momentum returns to its initial value after one full orbital period.

The last step is to express l^2 in terms of its orbit-averaged value, \bar{l}^2 . The latter can be obtained by averaging either Eq. (4.12) or (4.13):

$$\bar{l}^2 = l_0^2 + \frac{1}{2c^2} \frac{s_p^2}{\tilde{l}^2} (3 + 4e) \cos 2\phi_s = \tilde{l}^2 - \frac{1}{c^2} \left[2\nu (\mathbf{s}_1 \cdot \mathbf{s}_2) h + \frac{s_p^2}{2\tilde{l}^2} (1 - e^2 + e^2 \cos 2\phi_s) \right]. \quad (4.14)$$

Using this orbit-averaged value, l^2 can finally be decomposed as

$$l^2 = \bar{l}^2 - \frac{1}{2c^2} \frac{s_p^2}{\tilde{l}^2} [3e \cos(\phi - 2\phi_s) + 3 \cos(2\phi - 2\phi_s) + e \cos(3\phi - 2\phi_s)]. \quad (4.15)$$

We note that l^2, \tilde{l}^2, l_0^2 , and \bar{l}^2 all differ only by a 2PN quantity. Eq. (4.15) shows that l consists of a slowly varying secular component \bar{l} plus rapidly oscillating harmonics at integer multiples of the orbital frequency. While the structure of this decomposition was previously obtained by Ref. [41, 42], here we have provided a different derivation. Finally, substituting Eq. (4.15) into the coefficients (4.6), we obtain

$$C = -\bar{l}^2 + \frac{1}{c^2} [5(\nu - 2) + 2(1 - 3\nu) h \bar{l}^2 + \frac{s_p^2}{2\tilde{l}^2} (3e \cos(\phi - 2\phi_s) + 3 \cos(2\phi - 2\phi_s) + e \cos(3\phi - 2\phi_s))] + \frac{1}{c^4} [(37 - 122\nu + 36\nu^2) h - 3(1 - 5\nu + 5\nu^2) h^2 \bar{l}^2], \quad (4.16a)$$

$$D_1 = \frac{1}{c^2} [(8 - 3\nu) \bar{l}^2 - 2\mathbf{l} \cdot \mathbf{s}_{\text{eff}} + \mathcal{S}^2 - 3s_p^2 \cos^2(\phi - \phi_s)] + \frac{1}{c^4} \left[\frac{53}{2} - \frac{83\nu}{2} + 10\nu^2 - (16 - 73\nu + 19\nu^2) h \bar{l}^2 \right]. \quad (4.16b)$$

For the remaining coefficients (A , B , D_2 , and D_3), l can be replaced by its orbit-averaged counterpart \bar{l} , as the resulting differences contribute only at orders beyond 2PN. This completes the derivation of the radial equation of motion. We stress that the hybrid spin sector solution was not needed for the above manipulations, meaning that the radial equation of motion is 2PN accurate.

B. Azimuthal equation of motion

We now derive the EOM for the azimuthal angle ϕ of \mathbf{r} (measured from the unit vector \mathbf{i}) in the orbital plane perpendicular to \mathbf{l} , following the approach of Ref. [34]. The derivation requires expressing the orbital angular momentum vector $\mathbf{l} = \mathbf{r} \times \mathbf{p}$ in the NIF, obtained via the Euler Matrix in Eq (3.22). The separation vector in the NIF is given by

$$\mathbf{r} = r \begin{bmatrix} \cos \phi \\ \sin \phi \\ 0 \end{bmatrix}_{\text{NIF}}. \quad (4.17)$$

To express the canonical momentum \mathbf{p} in the NIF, we start from Hamilton's equations of motion

$$\frac{d\mathbf{r}}{dt} = \frac{\partial h}{\partial \mathbf{p}}. \quad (4.18)$$

Inverting this relation to express \mathbf{p} in terms of $\dot{\mathbf{r}}$ up to 2PN order, as detailed in Appendix F, yields

$$\mathbf{p} = \dot{\mathbf{r}} + \frac{1}{2c^2} \left[(1 - 3\nu) p^2 \dot{\mathbf{r}} + \frac{2}{r} \left(\nu (\mathbf{n} \cdot \mathbf{p}) \mathbf{n} + (3 + \nu) \dot{\mathbf{r}} \right) + \frac{2}{r^2} (\mathbf{n} \times \mathbf{s}_{\text{eff}}) \right]$$

$$\begin{aligned}
& + \frac{1}{8c^4} \left[(-1 + 3\nu + 3\nu^2)p^4 \dot{\mathbf{r}} + \frac{8}{r^2} \left(\nu^2(\mathbf{n} \cdot \mathbf{p})\mathbf{n} + (4 - 2\nu + \nu^2)\dot{\mathbf{r}} \right) \right. \\
& \left. + \frac{4}{r} \left((1 + 4\nu - 3\nu^2)p^2 \dot{\mathbf{r}} + \nu(1 - 2\nu)(\mathbf{n} \cdot \mathbf{p})p^2 \mathbf{n} + \nu^2(\mathbf{n} \cdot \mathbf{p})^2 \dot{\mathbf{r}} + 3\nu^2(\mathbf{n} \cdot \mathbf{p})^3 \mathbf{n} \right) \right] + \mathcal{O}\left(\frac{1}{c^5}\right). \quad (4.19)
\end{aligned}$$

The derivative of \mathbf{r} in the NIF becomes¹³

$$\dot{\mathbf{r}} = \begin{bmatrix} \dot{r} \cos \phi - r \sin \phi (\dot{\phi}_L \cos \theta_L + \dot{\phi}) \\ \dot{r} \sin \phi + r \cos \phi (\dot{\phi}_L \cos \theta_L + \dot{\phi}) \\ r(-\dot{\phi}_L \sin \theta_L \cos \phi + \dot{\theta}_L \sin \phi) \end{bmatrix}_{\text{NIF}}. \quad (4.20)$$

This expression, together with Eq. (4.3), completes the determination of \mathbf{p} in the NIF, providing the foundation for deriving the evolution of the azimuthal angle of the orbital separation vector \mathbf{r} . We start by writing the orbital angular momentum in the NIF

$$\mathbf{l}_{\text{NIF}} = \mathbf{r}_{\text{NIF}} \times \mathbf{p}_{\text{NIF}}, \quad (4.21)$$

with the z -component equal to l by construction.

By substituting Eqs. (3.24) and (4.17)–(4.20) into Eq. (4.21) and isolating $d\phi/dt$, we obtain

$$\begin{aligned}
\frac{d\phi}{dt} = & \frac{lr + \frac{1}{c^2}(\delta_1 s_1 \cos \kappa_1 + \delta_2 s_2 \cos \kappa_2)}{r^3 + \frac{r^2}{2c^2}[2(3 + \nu) + (1 - 3\nu)p^2 r] - \frac{1}{8c^4}[4\nu^2 l^2 - 8(4 - 2\nu + \nu^2)r - 4(1 + 4\nu - 2\nu^2)p^2 r^2 + (1 - 3\nu - 3\nu^2)p^4 r^3]} \\
& - \cos \theta_L \frac{d\phi_L}{dt}. \quad (4.22)
\end{aligned}$$

The azimuthal equation of motion, Eq. (4.22), is derived directly from the full 2PN dynamics and does not rely on any hybrid approximation. However, obtaining an explicit solution requires expressing the right-hand side in terms of quantities for which closed-form expressions are available. This is achieved by substituting the hybrid solutions for $\cos \theta_L$ and $d\phi_L/dt$ from Eqs. (3.23) and (3.26), with the replacement $d^{-3} \rightarrow r^{-3}$. As a consequence of this substitution, Σ_2 and λ , which under the full 2PN dynamics are not conserved, are treated as constants, consistent with the hybrid prescription. All quantities in the first term of Eq. (4.22), including the orbital angular momentum magnitude l , are kept at their exact 2PN values. Thus, the hybrid approximation is introduced only to model the geometric precession of the non-inertial frame, thereby enabling an explicit solution. Under these substitutions, $d\phi/dt$ reduces, via Eqs. (3.23), (4.2), and (4.3), to an expression involving only $\cos \kappa_1$ and a polynomial in $1/r$, which can then be integrated explicitly using an ansatz

$$\frac{d\phi}{dt} = \frac{F}{r^2} + \frac{I_{1o} + I_{1s}}{r^3} + \frac{I_2}{r^4} + \frac{I_3}{r^5} + \frac{1}{c^2 r^3} \left(\frac{\beta_{1L}}{\alpha_{1L} + \cos \kappa_1^{(2,H)}} + \frac{\beta_{2L}}{\alpha_{2L} + \cos \kappa_1^{(2,H)}} \right), \quad (4.23)$$

with coefficients

$$F = l + \frac{1}{c^2}(3\nu - 1)h\bar{l} + \frac{1}{2c^4}(2 - 9\nu + 6\nu^2)h^2\bar{l}, \quad (4.24a)$$

$$I_{1o} = \frac{2}{c^2}(\nu - 2)\bar{l} + \frac{2}{c^4}(2 - 11\nu + 4\nu^2)h\bar{l}, \quad (4.24b)$$

$$I_{1s} = -\frac{1}{2c^2} \left[(2\delta_1 + 2\delta_2 - \nu)(1 - \lambda)\bar{l} + \lambda(\nu\bar{l} - \frac{3\mu}{m_2}s_2\Sigma_2) \right], \quad (4.24c)$$

$$I_2 = \frac{1}{2c^4}(17 - 22\nu + 10\nu^2)\bar{l}, \quad (4.24d)$$

$$I_3 = \frac{1}{2c^4}\nu(1 - 2\nu)\bar{l}^3. \quad (4.24e)$$

The final term in Eq. (4.23), arising from spin precession, reflects that the orbital phase ϕ is measured with respect to the i -axis of the NIF, which itself precesses relative to the IF. The presence of $1/r^3$ in this term, rather than its

¹³Starting with Eq. (4.17), we first write \mathbf{r} in the IF with an Euler matrix transformation (Eq. (3.22)) take time derivative of the resulting components and then transform them back to the NIF using the reverse Euler matrix transformation.

orbit-averaged counterpart $1/d^3$, results from employing the hybrid prescription for $d\phi_L/dt$. The coefficients α_{iL} and β_{iL} entering in this term are defined in Eq. (3.27).

We now examine the time dependence of the coefficients in Eq. (4.23). The coefficients I_{1o} , I_2 and I_3 are at least at 1PN order so the oscillations of l can be neglected, making them effectively constant over an orbital period, analogously to D_{1o} , D_2 and D_3 in Eq. (4.6). The spin-dependent term I_{1s} arises from the hybrid approximation and involves only slow variables, so it can be considered as constant on the orbital timescale. However F depends on l^2 at Newtonian order, therefore its 2PN oscillations cannot be neglected and F is analogous to the coefficient C in Eq. (4.16).

In this formulation, the hybrid approximation is restricted to the spin-precession term and the quantities entering it, ensuring that the remaining coefficients and dynamics remain 2PN accurate. In the following subsection, we construct a quasi-Keplerian parametrization of the vector \mathbf{R} in the NIF by finding a solution that simultaneously satisfies Eqs. (4.4) and (4.23).

C. Quasi-Keplerian parametrization of \mathbf{R}

Unlike the non-spinning case treated by Wex and Schäfer in Ref. [30] or the spin-orbit case by Cho and Lee in Ref. [34], a direct integration of Eqs. (4.4) and (4.23) is not possible because some coefficients vary on the orbital timescale. We therefore follow the ansatz-based approach introduced by Klein in Ref. [42], constructing a parametric solution involving generalized Keplerian elements with free parameters that are fixed by requiring the ansatz to satisfy the equations of motion. The key constraint is that the resulting orbital elements must remain constant on the orbital timescale (though they may vary on the longer precessional timescale). A detailed harmonic analysis justifying the functional form of our ansatz is presented in Appendix G. The resulting quasi-Keplerian parametrization that satisfies Eqs. (4.4) and (4.23) is

$$n(t - t_0) = u - e_t \sin u + \frac{1}{c^4} [f_t \sin v_\phi + g_t (v_\phi - u)], \quad (4.25a)$$

$$r = a_r(1 - e_r \cos u) + \frac{1}{c^2} h_r \cos(2v_\phi - 2\phi_s), \quad (4.25b)$$

$$v_\phi = u + 2 \arctan \left(\frac{\beta_\phi \sin u}{1 - \beta_\phi \cos u} \right), \quad \text{with } \beta_\phi = \frac{e_\phi}{1 + \sqrt{1 - e_\phi^2}}, \quad (4.25c)$$

$$\phi(t) - \phi(t_0) = (1 + \tilde{k})v_\phi + \frac{1}{c^4} [f_\phi \sin 2v_\phi + g_\phi \sin 3v_\phi] + \frac{1}{c^2} [h_{\phi 1} \sin(v_\phi - 2\phi_s) + h_{\phi 2} \sin(2v_\phi - 2\phi_s)] + \Pi_k(u), \quad (4.25d)$$

where

$$\Pi_k(u) \equiv \frac{2}{\sqrt{A(x_3 - x_-)}} \sum_{i=1}^2 \frac{\beta_{iL}}{\alpha_{iL} + x_-} \Pi \left(\frac{x_- - x_+}{\alpha_{iL} + x_-}, \text{am}(\Upsilon(u), \beta), \beta \right). \quad (4.26)$$

The quasi-Keplerian parameters are given by

$$n = (-2h)^{3/2} \left[1 + \frac{1}{4c^2} (15 - \nu) h + \frac{1}{c^4} \left(\frac{3}{2} (-5 + 2\nu) \frac{(-2h)^{3/2}}{\bar{l}} + \frac{1}{32} (555 + 30\nu + 11\nu^2) h^2 \right) \right], \quad (4.27a)$$

$$e_t^2 = 1 + 2h\bar{l}^2 + \frac{1}{c^2} \left[4(1 - \nu)h + (17 - 7\nu)h^2\bar{l}^2 + \frac{h}{\bar{l}^2} (4\mathbf{l} \cdot \mathbf{s}_{\text{eff}} - 2\mathcal{S}^2 + 3s_p^2) \right] \quad (4.27b)$$

$$+ \frac{1}{c^4} \left[(11\nu - 17) \frac{h}{\bar{l}^2} + 2(2 + \nu + 5\nu^2)h^2 + (112 - 47\nu + 16\nu^2)h^3\bar{l}^2 + 3(2\nu - 5)(1 + 2h\bar{l}^2) \frac{(-2h)^{3/2}}{\bar{l}} \right], \quad (4.27c)$$

$$f_t = -\frac{1}{8}\nu(4 + \nu)\sqrt{1 + 2h\bar{l}^2} \frac{(-2h)^{3/2}}{\bar{l}}, \quad (4.27d)$$

$$g_t = \frac{3}{2}(5 - 2\nu) \frac{(-2h)^{3/2}}{\bar{l}}, \quad (4.27e)$$

$$a_r = -\frac{1}{2h} \left[1 + \frac{1}{2c^2} h \left((7 - \nu) - \frac{1}{\bar{l}^2} (4\mathbf{l} \cdot \mathbf{s}_{\text{eff}} - 2\mathcal{S}^2 + 3s_p^2) \right) + \frac{1}{4c^4} \left(2(17 - 11\nu) \frac{h}{\bar{l}^2} + (1 + 10\nu + \nu^2) h^2 \right) \right], \quad (4.27f)$$

$$e_r^2 = 1 + 2h\bar{l}^2 - \frac{1}{c^2} \left[2(6 - \nu)h + 5(3 - \nu)h^2\bar{l}^2 - 2\frac{h}{\bar{l}^2}(1 + h\bar{l}^2)(4\mathbf{l} \cdot \mathbf{s}_{\text{eff}} - 2\mathcal{S}^2 + 3s_p^2) \right] + \frac{1}{c^4} \left[-2(17 - 11\nu)\frac{h}{\bar{l}^2} + (26 + \nu + \nu^2)h^2 + (80 - 55\nu + 4\nu^2)h^3\bar{l}^2 \right], \quad (4.27g)$$

$$h_r = -\frac{s_p^2}{4\bar{l}^2}, \quad (4.27h)$$

$$e_\phi^2 = 1 + 2h\bar{l}^2 + \frac{1}{c^2}h \left[-(12 - 4\Delta) - (15 - \nu - 8\Delta)h\bar{l}^2 + \frac{1}{\bar{l}^2}(3 + 4h\bar{l}^2)(4\mathbf{l} \cdot \mathbf{s}_{\text{eff}} - 2\mathcal{S}^2 + 3s_p^2) - 2(1 + 2h\bar{l}^2)\lambda \left((2\Delta - \nu) + 3\frac{s_2}{\bar{l}}\frac{\mu}{m_2}\Sigma_2 \right) \right] + \frac{1}{c^4} \left[\frac{1}{8} \left(-408 + 232\nu + 15\nu^2 + 64\Delta \left(4 - \frac{5}{2}\nu + \Delta \right) \right) \frac{h}{\bar{l}^2} - \frac{1}{2} \left(16 - 88\nu - 9\nu^2 - 12\Delta \left(1 - 9\nu + \frac{14}{3}\Delta \right) \right) h^2 + \frac{1}{2} \left(160 - 30\nu + 3\nu^2 - 16\Delta(10 + 3\nu - 3\Delta) \right) h^3\bar{l}^2 \right] \quad (4.27i)$$

$$\tilde{k} = \frac{1}{c^2\bar{l}^2} \left[3 - \Delta - \frac{3}{4\bar{l}^2}(4\mathbf{l} \cdot \mathbf{s}_{\text{eff}} - 2\mathcal{S}^2 + 3s_p^2) + \frac{1}{2}\lambda \left((2\Delta - \nu) + 3\frac{s_2}{\bar{l}}\frac{\mu}{m_2}\Sigma_2 \right) + \frac{1}{4c^2\bar{l}^2} \left(105 - 30\nu - 60\Delta + 15\Delta\nu - 2h\bar{l}^2(-15 + 6\nu + \Delta(18 - 13\nu)) \right) \right], \quad (4.27j)$$

$$f_\phi = \frac{1}{8}(\nu - 3\nu^2 - \Delta(8 - 5\nu + 2\Delta))(1 + 2h\bar{l}^2)\frac{1}{\bar{l}^4}, \quad (4.27k)$$

$$g_\phi = -\frac{3\nu^2}{32}(1 + 2h\bar{l}^2)^{3/2}\frac{1}{\bar{l}^4}, \quad (4.27l)$$

$$h_{\phi 1} = -\frac{1}{2}\sqrt{1 + 2h\bar{l}^2}\frac{s_p^2}{\bar{l}^4}, \quad (4.27m)$$

$$h_{\phi 2} = -\frac{s_p^2}{8\bar{l}^4}. \quad (4.27n)$$

Here, we have defined the mass term $\Delta \equiv \delta_1 + \delta_2 - \nu/2$. Interestingly, although Δ originates strictly from spin-orbit and spin-spin couplings, it enters the azimuthal equation of motion (4.23) at the 1PN order through the coefficient I_{1s} . This scaling allows it to couple directly with the 1PN non-spinning orbital terms, generating novel 2PN cross-contributions in the azimuthal quasi-Keplerian parameters (Eq. (4.25d)). This orbital-spin coupling represents a qualitative departure from the 1.5PN dynamics, where the non-spinning and spin-orbit contributions remain strictly independent and linearly additive. At 2PN order, this independence breaks down in the azimuthal sector, necessitating a unified mathematical treatment of the spin and orbital terms. Furthermore, because of the 2PN spin-spin dynamics, the quasi-Keplerian parameters that depend explicitly on \mathcal{S} or $\mathbf{l} \cdot \mathbf{s}_{\text{eff}}$ are no longer strictly constant, but instead exhibit slow secular variations.

We highlight a subtle but physically significant distinction between the azimuthal parameter \tilde{k} appearing in Eq. (4.25d) and the standard periastron advance k found in much of the literature (e.g., Refs. [27, 30]). Physically, \tilde{k} is closely related to the periastron advance measured purely within the orbital plane; it would exactly match the standard periastron advance k if the precessional rate $\dot{\phi}_L$ in Eq. (4.22) were artificially set to zero. However, due to this precession, the x -axis of the non-inertial frame rotates relative to the inertial frame. Because the precession of the orbital angular momentum \mathbf{L} continuously modifies the reference axis from which the azimuthal phase of \mathbf{R} is measured, it induces an additional secular drift. This effect is mainly encapsulated by the incomplete elliptic integrals in Eq. (4.25d). These integrals decompose into a steady secular growth and a bounded oscillatory correction. To extract the total secular advance, we first integrate over the 1PN radial orbit, which eliminates all oscillatory contributions and isolates the terms associated with v_r , entering through the hybrid argument $\Upsilon^{(2,H)}$ in Eq. (3.44b). We then integrate over one nutation period and rescale the result accordingly (see Eq. (I.1)). This procedure yields the effective periastron advance k , properly incorporating the cumulative precession of the reference frame as an additional secular term. It gives

$$k \equiv \tilde{k} + \frac{1}{nc^2a^3} \left[\frac{\beta_{1L}}{\alpha_{1L} + x_-} \frac{\Pi(n_1, \beta)}{K(\beta)} + \frac{\beta_{2L}}{\alpha_{2L} + x_-} \frac{\Pi(n_2, \beta)}{K(\beta)} \right], \quad (4.28)$$

where the elliptic characteristics are defined as $n_i = \frac{x_- - x_+}{\alpha_{iL} + x_-}$. Here, $\Pi(n_i, \beta)$ and $K(\beta)$ denote the complete elliptic integrals of the third and first kind, respectively. Together with the radial mean motion n and the slow frequencies governing nutation and precession, the effective periastron advance k completes the set of variables required to span the four fundamental frequencies of the phase space (see Appendix I).

Our complete quasi-Keplerian parametrization smoothly reduces to the spin-aligned configuration of Ref. [27], as explicitly demonstrated in Appendix H. In the strict spin-aligned limit ($\kappa_1, \kappa_2, \gamma, s_p \rightarrow 0$), all supplementary 2PN oscillatory functions naturally vanish, allowing the radial and temporal parameters to identically match the established non-precessing literature. In the azimuthal sector, however, at first sight, a direct comparison of the non-inertial orbital phase $\phi(t)$ from Eq. (4.25d) to the aligned-spin literature yields apparent deviations in the orbital elements k , e_ϕ , f_ϕ , and g_ϕ . As shown in Appendix H, the observable azimuthal phase in the inertial frame is given by the sum $\Phi_{\text{spin-aligned}} = \phi + \phi_L$. Combining these two angles, taking the spin-aligned limit, and expressing the result in terms of a redefined true anomaly yields exactly the quasi-Keplerian parametrization Eq (H.10), derived in Ref. [27]. This demonstrates that integrating the precessing equations of motion and subsequently taking the spin-aligned limit is a mathematically consistent, commuting procedure.

In the quasi-circular limit ($e_t \rightarrow 0$), our results match the findings of Refs. [42, 43]. Due to the 2PN spin-spin interaction, specifically the terms h_r , $h_{\phi 1}$, and $h_{\phi 2}$, neither the distance r nor the angular speed $\dot{\phi}$ can stay constant. Instead, the spins cause the orbit to have small fluctuations. These quantities only become constant if one performs an orbit-average to smooth out these fast, spin-spin driven wiggles.

Furthermore, by explicitly setting $\dot{\phi}_L = 0$ in Eq. (4.22) and removing the orbital corrections, our formulation mathematically recovers the quasi-Keplerian parametrization of Ref. [42]. While the gauge-invariant secular advance agrees identically, the intermediate orbital elements naturally exhibit differences due to the respective coordinate choices (ADM versus harmonic) and spin supplementary conditions.

The Eqs. (4.25) and (4.27) constitute our complete 2PN quasi-Keplerian solution for spinning binaries on eccentric orbits. The solution is valid for arbitrary mass ratios, spin magnitudes, spin orientations, and eccentricities (provided the orbit remains bound, i.e., $e < 1$) as long as we remain within the PN approximation.

5. CONCLUDING REMARKS

A. Scope and novelty of the present work

The primary objective of this work was to provide an analytical description of the conservative dynamics of eccentric and precessing binary black hole systems at the 2PN order. Working within the ADM Hamiltonian framework with the NWP spin supplementary condition, we have extended the 1.5PN solution of Ref. [34] to 2PN order. Our main contributions can be summarized as follows

- **Hybrid 2PN spin solution:** We have developed a hybrid analytical solution for the spin evolution that incorporates nearly all conservative effects through 2PN order, including non-spinning corrections, 1.5PN spin-orbit coupling, and 2PN long timescale spin-spin interactions. By introducing the hybrid precession velocity $\Omega^{(2,H)}$ in Eq. (3.41), we capture both the 2PN accurate slow evolution and the fast leading-order 1.5PN oscillations. The only missing ingredient are the sub-dominant 2PN spin-spin induced fast orbital timescale oscillations. The spin dynamics is encapsulated in the final solution of $\cos \kappa_1^{(2,H)}$ in Eq. (3.44a).
- **2PN orbital solution:** We derived a quasi-Keplerian parametrization for the relative separation vector \mathbf{R} , providing explicit solutions for the radial motion $R(t)$ and the phase $\phi(t)$, given in Eq. (4.25), where the radial solution is fully 2PN accurate while the phase omits only the 2PN spin-spin oscillations arising from spin evolution. To ensure an observable solution, we consistently tracked the rotation of the non-inertial frame relative to the fixed inertial frame via time-dependent Euler angles $\theta_L(t)$ and $\phi_L(t)$, keeping the total azimuthal phase well-defined at all times. Interestingly at 2PN order, the non-spinning and spinning sectors are coupled through products of 1PN terms, appearing in the azimuthal QKP parameters in Eq. (4.27), where the mass term Δ interacts with 1PN orbital contributions to produce novel 2PN cross-terms absent at lower orders. Finally in the spin-aligned limit, our general precessing QKP solution reduces to standard non-precessing dynamics, and it also remains consistent with the standard quasi-circular limit.

The analytical solution constructed in this article is implemented in a *Mathematica* notebook, `2PN_BBH_solution.nb`, hosted in our public GitHub repository [45].

B. Future perspectives

The analytical solution presented in this work is strictly conservative, describing the bound motion of the binary system under the 2PN Hamiltonian dynamics. A natural and necessary extension of this framework lies in the inclusion of dissipative effects, specifically the radiation-reaction contributions entering at 2.5PN order. They are responsible for the loss of energy and angular momentum of the binary system, driving the secular shrinking and circularization of the orbit.

Future work will therefore focus on deriving the secular time evolution of the quasi-Keplerian parameters due to radiation reaction. Once the time dependence of the orbital elements is established, one can compute the full gravitational wave signal. The resulting waveforms will be crucial for accurate parameter estimation, as they will consistently capture both the amplitude modulations induced by spin precession and the frequency chirping driven by radiation reaction.

ACKNOWLEDGMENTS

We thank Guillaume Faye, David Trestini, Soham Bhattacharyya, Thibault Damour, Quentin Henry and Leo Stein for useful discussions. LB acknowledges financial support from the ANR PRoGRAM project, grant ANR-21-CE31-0003-001. LB, TC and ST acknowledge financial support from the EU Horizon 2020 Research and Innovation Programme under the Marie Skłodowska-Curie Grant Agreement no.101007855. ST was supported by the PSL postdoctoral fellowship during this work.

Appendix A: Triple product of angular momenta

The scalar triple product $\mathbf{l} \cdot (\mathbf{s}_1 \times \mathbf{s}_2)$ can be expressed in terms of the characteristic angles of the system. Using the geometric properties of the three angular momentum vectors, we obtain

$$\mathbf{l} \cdot (\mathbf{s}_1 \times \mathbf{s}_2) = l s_1 s_2 \sin \kappa_1 \sin \kappa_2 \sin \Delta\phi_s, \quad (\text{A.1})$$

where $\Delta\phi_s \equiv \phi_{s_2} - \phi_{s_1}$ denotes the difference between the azimuthal angles of the two spin vectors projected onto the orbital plane, with ϕ_{s_a} defined in Eq. (3.24).

The derivation of Eq. (3.15) requires the following auxiliary relation between the angles

$$\cos \Delta\phi_s = \frac{\cos \gamma - \cos \kappa_1 \cos \kappa_2}{\sin \kappa_1 \sin \kappa_2}, \quad (\text{A.2})$$

which follows from the spherical law of cosines applied to the angular momentum triangle.

Appendix B: Roots of the cubic polynomial

We compute the roots of the cubic polynomial appearing in Eq. (3.17) following the approach of Appendix A.1 in Ref. [53]. The polynomial reads

$$P(x) = a_3 x^3 + a_2 x^2 + a_1 x + a_0, \quad (\text{B.1})$$

with coefficients

$$a_3 = 2 m_2 (m_1 - m_2) l s_1, \quad (\text{B.2a})$$

$$a_2 = -\left((m_1 - m_2)^2 l^2 + m_2^2 s_1^2 + m_1^2 s_2^2 + 2 m_1 m_2 s_1 s_2 \Sigma_1 + 2 m_1 (m_1 - m_2) l s_2 \Sigma_2 \right), \quad (\text{B.2b})$$

$$a_1 = 2 m_1 s_2 \left((m_1 - m_2) l \Sigma_1 + (m_2 s_1 + m_1 s_2 \Sigma_1) \Sigma_2 \right), \quad (\text{B.2c})$$

$$a_0 = m_1^2 s_2^2 (1 - \Sigma_1^2 - \Sigma_2^2). \quad (\text{B.2d})$$

Note that $a_3 = A$ of Eq. (3.18) and is positive since $m_1 > m_2$ by convention. The polynomial factorizes as

$$P(x) = a_3 (x - x_-)(x - x_+)(x - x_3). \quad (\text{B.3})$$

To obtain the roots analytically, we perform the standard depressed cubic transformation via the change of variables

$$y \equiv x + \frac{a_2}{3a_3}, \quad (\text{B.4})$$

which eliminates the quadratic term and yields the reduced polynomial

$$P(x) \equiv Q(y) = a_3(y^3 + py + q), \quad (\text{B.5})$$

where the reduced coefficients are

$$p = \frac{3a_1a_3 - a_2^2}{3a_3^2}, \quad (\text{B.6a})$$

$$q = \frac{2a_2^3 - 9a_1a_2a_3 + 27a_0a_3^2}{27a_3^3}. \quad (\text{B.6b})$$

The discriminant of the depressed cubic is $\Delta = -4p^3 - 27q^2$. When $\Delta > 0$, all three roots are real and distinct, which corresponds to $p < 0$. In this regime, the roots can be expressed using the trigonometric formulation

$$x_k = -\frac{a_2}{3a_3} + 2\sqrt{\frac{-p}{3}} \cos \left[\frac{1}{3} \arccos \left(\frac{3q}{2p} \sqrt{\frac{-3}{p}} \right) + \delta_k \right], \quad (\text{B.7})$$

for $k \in \{-, +, 3\}$, with the corresponding phase shifts $\delta_3 = 0$, $\delta_- = 2\pi/3$, and $\delta_+ = 4\pi/3$. This expression is valid when the argument of the arccosine lies in $[-1, 1]$, which is guaranteed by the condition $\Delta > 0$. Modifying the convention of Ref. [34], these solutions naturally yield the ordering $x_- \leq x_+ < x_3$.

In the PN regime, where $s_a/l \sim \mathcal{O}(c^{-1})$, the three roots exhibit distinct behaviors. The largest root scales as

$$x_3 \sim \frac{m_1 - m_2}{6m_2} \frac{l}{s_1} \sim \mathcal{O}(c), \quad (\text{B.8})$$

placing it outside the physical interval $[-1, 1]$. The other two roots remain finite and nearly degenerate. They scale as

$$x_{\pm} = \cos \kappa_1 + \frac{m_1}{m_1 - m_2} \frac{s_2}{l} (\cos \gamma - \cos \kappa_1 \cos \kappa_2 \pm |\sin \kappa_1 \sin \kappa_2|) + \mathcal{O}(c^{-2}) \quad (\text{B.9})$$

and both are physically relevant. Their splitting

$$x_+ - x_- \sim \frac{2m_1}{m_1 - m_2} \frac{s_2}{l} |\sin \kappa_1 \sin \kappa_2| \sim \mathcal{O}(c^{-1}) \quad (\text{B.10})$$

determines the nutation amplitude and $\cos \kappa_1$ oscillates between these two values during each nutation cycle, as it can be seen from Eq. (3.19).

Appendix C: Azimuthal equation of motion of the orbital angular momentum

We project the definition of the total angular momentum $\mathbf{j} = \mathbf{l} + \mathbf{s}_1 + \mathbf{s}_2$ onto the three orthogonal directions of the non-inertial frame. Using the vector decomposition given in Eq. (3.24), we obtain

$$0 = s_1 \sin \kappa_1 \cos \phi_{s_1} + s_2 \sin \kappa_2 \cos \phi_{s_2}, \quad (\text{C.1a})$$

$$j \sin \theta_L = s_1 \sin \kappa_1 \sin \phi_{s_1} + s_2 \sin \kappa_2 \sin \phi_{s_2}, \quad (\text{C.1b})$$

$$j \cos \theta_L = l + s_1 \cos \kappa_1 + s_2 \cos \kappa_2. \quad (\text{C.1c})$$

Substituting Eq. (3.14) into Eq. (C.1c), we can express $\cos \theta_L$ as a function of $\cos \kappa_1$

$$\cos \theta_L = \frac{l + s_2 \Sigma_2}{j} + \frac{m_1 - m_2}{m_1} \frac{s_1}{j} \cos \kappa_1. \quad (\text{C.2})$$

Similarly, from Eqs. (C.1a) and (C.1b), we derive the azimuthal angle ϕ_{s_1} in terms of the other geometric variables

$$\sin \phi_{s_1} = \frac{s_1 \sin \kappa_1 + s_2 \sin \kappa_2 \cos \Delta \phi_s}{j \sin \theta_L}, \quad (\text{C.3a})$$

$$\cos \phi_{s_1} = \frac{s_2 \sin \kappa_2 \sin \Delta \phi_s}{j \sin \theta_L}. \quad (\text{C.3b})$$

These are all the relationships we need to obtain Eq. (3.26).

Appendix D: Analytical error bounds between the solutions

In this appendix, we compute analytical error bound between the three analytical solutions and the full 2PN one. We define the difference between two spin evolutions by the error vector

$$\boldsymbol{\delta}^{XY}(t) \equiv \mathbf{s}_1^X(t) - \mathbf{s}_1^Y(t), \quad X, Y \in \{(1.5), (2), (2, A), (2, H)\}, \quad (\text{D.1})$$

where $\mathbf{s}_1^X(t)$ denotes the spin vector evolved with the angular velocity $\boldsymbol{\Omega}^X$, as specified in Eqs. (3.38)–(3.41). Differentiating Eq. (D.1) with respect to time, we get

$$\frac{d}{dt} \boldsymbol{\delta}^{XY} = \boldsymbol{\Omega}^X \times \boldsymbol{\delta}^{XY} + (\boldsymbol{\Omega}^X - \boldsymbol{\Omega}^Y) \times \mathbf{s}_1^Y. \quad (\text{D.2})$$

Taking the time derivative of $\|\boldsymbol{\delta}^{XY}\|$ and using the antisymmetry of the cross product, the term proportional to $\boldsymbol{\Omega}^X \times \boldsymbol{\delta}^{XY}$ drops out, giving

$$\begin{aligned} \frac{d}{dt} \|\boldsymbol{\delta}^{XY}\| &= \frac{\boldsymbol{\delta}^{XY} \cdot \dot{\boldsymbol{\delta}}^{XY}}{\|\boldsymbol{\delta}^{XY}\|} \\ &= \frac{\boldsymbol{\delta}^{XY} \cdot ((\boldsymbol{\Omega}^X - \boldsymbol{\Omega}^Y) \times \mathbf{s}_1^Y)}{\|\boldsymbol{\delta}^{XY}\|}. \end{aligned} \quad (\text{D.3})$$

Integrating Eq. (D.3) from 0 to $t = N\tau_{\text{orb}} + \delta t$, with $N = \lfloor t/\tau_{\text{orb}} \rfloor$, and decomposing the interval into complete orbital periods yields

$$\begin{aligned} \|\boldsymbol{\delta}^{XY}(t)\| &= \sum_{k=0}^{N-1} \int_{k\tau_{\text{orb}}}^{(k+1)\tau_{\text{orb}}} \frac{\boldsymbol{\delta}^{XY}(\tau)}{\|\boldsymbol{\delta}^{XY}(\tau)\|} \cdot [(\boldsymbol{\Omega}^X(\tau) - \boldsymbol{\Omega}^Y(\tau)) \times \mathbf{s}_1^Y(\tau)] d\tau \\ &+ \int_{N\tau_{\text{orb}}}^t \frac{\boldsymbol{\delta}^{XY}(\tau)}{\|\boldsymbol{\delta}^{XY}(\tau)\|} \cdot [(\boldsymbol{\Omega}^X(\tau) - \boldsymbol{\Omega}^Y(\tau)) \times \mathbf{s}_1^Y(\tau)] d\tau. \end{aligned} \quad (\text{D.4})$$

Over a single orbital period, the variables \mathbf{l} and \mathbf{s}_a evolve on timescales much longer than τ_{orb} and may therefore be treated as constant. Evaluating $\boldsymbol{\delta}^{XY}$ and \mathbf{s}_1^Y at the beginning of each interval then gives

$$\begin{aligned} \|\boldsymbol{\delta}^{XY}(t)\| &= \sum_{k=0}^{N-1} \frac{\boldsymbol{\delta}^{XY}(k\tau_{\text{orb}})}{\|\boldsymbol{\delta}^{XY}(k\tau_{\text{orb}})\|} \cdot \left[\left(\int_{k\tau_{\text{orb}}}^{(k+1)\tau_{\text{orb}}} \boldsymbol{\Omega}^X(\tau) - \boldsymbol{\Omega}^Y(\tau) d\tau \right) \times \mathbf{s}_1^Y(k\tau_{\text{orb}}) \right] \\ &+ \frac{\boldsymbol{\delta}^{XY}(N\tau_{\text{orb}})}{\|\boldsymbol{\delta}^{XY}(N\tau_{\text{orb}})\|} \cdot \left[\left(\int_{N\tau_{\text{orb}}}^t \boldsymbol{\Omega}^X(\tau) - \boldsymbol{\Omega}^Y(\tau) d\tau \right) \times \mathbf{s}_1^Y(N\tau_{\text{orb}}) \right]. \end{aligned} \quad (\text{D.5})$$

Applying the Cauchy–Schwarz inequality and using $\|\mathbf{a} \times \mathbf{b}\| \leq \|\mathbf{a}\| \|\mathbf{b}\|$, we obtain the general error estimate

$$\|\boldsymbol{\delta}^{XY}(t)\| \leq s_1 \sum_{k=0}^{N-1} \left\| \int_{k\tau_{\text{orb}}}^{(k+1)\tau_{\text{orb}}} \boldsymbol{\Omega}^X(\tau) - \boldsymbol{\Omega}^Y(\tau) d\tau \right\| + s_1 \left\| \int_{N\tau_{\text{orb}}}^t \boldsymbol{\Omega}^X(\tau) - \boldsymbol{\Omega}^Y(\tau) d\tau \right\|, \quad (\text{D.6})$$

where we used the conservation of the spin magnitude, $\|\mathbf{s}_1^Y\| = s_1$, which holds for all models with given identical initial conditions. The Eq. (D.6) serves as the basis of all subsequent comparisons.

It is convenient to decompose the spin-orbit and spin-spin angular velocities into orbit-averaged and oscillatory components

$$\tilde{\Omega}_{\text{SO,SS}} \equiv \Omega_{\text{SO,SS}} - \bar{\Omega}_{\text{SO,SS}}, \quad (\text{D.7})$$

where $\bar{\Omega}_{\text{SO,SS}}$ denotes the orbital average of $\Omega_{\text{SO,SS}}$ and $\tilde{\Omega}_{\text{SO,SS}}$ is a purely oscillatory contribution satisfying $\langle \tilde{\Omega}_{\text{SO,SS}} \rangle = 0$.

We now apply the bound (D.6) to compare the three approximate spin evolution models with the full 2PN dynamics. First, we recall the PN estimates: $s_1 \sim c^{-1}$, while $\Omega_{\text{SO}} \sim c^{-2}$ and $\Omega_{\text{SS}} \sim c^{-3}$. Then, a useful simplification is to replace all orbital and spin variables \mathbf{r} , \mathbf{l} , and \mathbf{s}_a entering Ω^X by their 1.5PN values, as model-dependent differences contribute only at a higher order to the spin error for $t \lesssim \mathcal{O}(\tau_{\text{prec}}^{3/2})$. Similarly, the orbit-averaged solution differ from 1.5PN by the removal of oscillatory components, but these oscillations are subleading and can also be replaced by the 1.5PN solution without affecting the leading-order bound. Thus, for the leading-order estimate, all variables inside Ω^X can consistently be evaluated using the shared 1.5PN solution. This approximation and its justification are discussed further after the computation of the three error bounds.

a. 1.5PN versus 2PN. We first specialize the general bound (D.6) to the difference between the 1.5PN and 2PN spin evolutions. Using the decomposition (D.7) and applying the triangle inequality to the orbital-period integrals, we obtain

$$\begin{aligned} \|\mathbf{s}_1^{(2)}(t) - \mathbf{s}_1^{(1.5)}(t)\| &\leq s_1 \sum_{k=0}^{N-1} \left\| \int_{k\tau_{\text{orb}}}^{(k+1)\tau_{\text{orb}}} \bar{\Omega}_{\text{SS}}(\tau) d\tau \right\| + s_1 \sum_{k=0}^{N-1} \left\| \int_{k\tau_{\text{orb}}}^{(k+1)\tau_{\text{orb}}} \tilde{\Omega}_{\text{SS}}(\tau) d\tau \right\| + s_1 \left\| \int_{N\tau_{\text{orb}}}^t \Omega_{\text{SS}}(\tau) d\tau \right\| \\ &\leq s_1 \sum_{k=0}^{N-1} \tau_{\text{orb}} \|\bar{\Omega}_{\text{SS}}(k\tau_{\text{orb}})\| + s_1 \left\| \int_{N\tau_{\text{orb}}}^t \Omega_{\text{SS}}(\tau) d\tau \right\| \end{aligned} \quad (\text{D.8})$$

In the second line, we have used the fact that by construction, the oscillatory component $\tilde{\Omega}_{\text{SS}}$ averages to zero over each orbital period, so the second sum vanishes identically. The remaining terms then give

$$\|\mathbf{s}_1^{(2)}(t) - \mathbf{s}_1^{(1.5)}(t)\| \leq \mathcal{O}\left(s_1 t \max_{\tau \leq t} \|\bar{\Omega}_{\text{SS}}(\tau)\|\right) = \mathcal{O}(t c^{-4}), \quad (\text{D.9})$$

indicating that the 1.5PN-2PN spin difference increases linearly with time due to the missing secular spin-spin effect.

b. 2PN averaged versus 2PN. We next compare the full 2PN spin evolution with its orbit-averaged counterpart. Using the same bound (D.6) and separating the contributions from the first term with the triangle inequality, we find

$$\|\mathbf{s}_1^{(2)}(t) - \mathbf{s}_1^{(2,A)}(t)\| \leq s_1 \sum_{k=0}^{N-1} \left\| \int_{k\tau_{\text{orb}}}^{(k+1)\tau_{\text{orb}}} \tilde{\Omega}_{\text{SO}}(\tau) d\tau \right\| + s_1 \sum_{k=0}^{N-1} \left\| \int_{k\tau_{\text{orb}}}^{(k+1)\tau_{\text{orb}}} \tilde{\Omega}_{\text{SS}}(\tau) d\tau \right\| + s_1 \left\| \int_{N\tau_{\text{orb}}}^t \tilde{\Omega}_{\text{SO}}(\tau) + \tilde{\Omega}_{\text{SS}}(\tau) d\tau \right\|. \quad (\text{D.10})$$

The first two sums vanish because both oscillatory components have zero orbital average. The only remaining contribution comes from the incomplete final orbital interval and is dominated by the spin-orbit coupling. Consequently, the accumulated error remains bounded as

$$\|\mathbf{s}_1^{(2)}(t) - \mathbf{s}_1^{(2,A)}(t)\| \leq \mathcal{O}\left(s_1 \delta t \max_{\tau \in [N\tau_{\text{orb}}, t]} \|\tilde{\Omega}_{\text{SO}}(\tau) + \tilde{\Omega}_{\text{SS}}(\tau)\|\right) = \mathcal{O}(c^{-3}), \quad (\text{D.11})$$

for times $t \lesssim \mathcal{O}(\tau_{\text{prec}}^{3/2})$.

c. 2PN hybrid versus 2PN. Finally, we compare the full 2PN spin evolution with the hybrid 2PN model. Applying the general bound (D.6) and separating the different contributions give

$$\begin{aligned} \|\mathbf{s}_1^{(2)}(t) - \mathbf{s}_1^{(2,H)}(t)\| &\leq s_1 \sum_{k=0}^{N-1} \left\| \int_{k\tau_{\text{orb}}}^{(k+1)\tau_{\text{orb}}} \tilde{\Omega}_{\text{SS}}(\tau) d\tau \right\| + s_1 \sum_{k=0}^{N-1} \|\bar{\Omega}_{\text{SS}}(k\tau_{\text{orb}})\| \left\| \int_{k\tau_{\text{orb}}}^{(k+1)\tau_{\text{orb}}} \left(1 - \frac{d^3}{r^3}\right) d\tau \right\| \\ &\quad + s_1 \left\| \int_{N\tau_{\text{orb}}}^t \tilde{\Omega}_{\text{SS}}(\tau) + \left(1 - \frac{d^3}{r^3}\right) \bar{\Omega}_{\text{SS}}(\tau) d\tau \right\|. \end{aligned} \quad (\text{D.12})$$

The first sum vanishes because $\tilde{\Omega}_{\text{SS}}$ has zero orbital average, while the second sum vanishes because the orbital average of r^{-3} equals d^{-3} . The only nonzero contribution arises from the subleading 2PN spin–spin oscillations, which the hybrid model reproduces incorrectly. This highlights that the hybrid model captures both the secular 2PN spin–spin precession and the leading-order oscillatory behavior, while only the subdominant oscillatory corrections are misrepresented. Consequently, the accumulated error is bounded and satisfies

$$\|\mathbf{s}_1^{(2)}(t) - \mathbf{s}_1^{(2,\text{H})}(t)\| \leq \mathcal{O}\left(s_1 \delta t \max_{\tau \in [N\tau_{\text{orb}}, t]} \left\| \tilde{\Omega}_{\text{SS}}(\tau) + \left(1 - \frac{d^3}{r^3}\right) \bar{\Omega}_{\text{SS}}(\tau) \right\|\right) = \mathcal{O}(c^{-4}). \quad (\text{D.13})$$

Altogether, these results reproduce the general error bound as stated in Eq. (3.45) and illustrated in Fig. 3.

A potential concern arises from our removal of the model labels for the vectors inside the angular velocities. In practice, this corresponds to setting to zero in Eq. (D.8) the difference between the spin–orbit angular velocities of the 1.5PN and 2PN models. We now show that this approximation introduces only a subleading error, which remains negligible for times $t \lesssim \mathcal{O}(\tau_{\text{prec}}^{3/2})$.

Because all models are initialized with identical orbital and spin configurations, the difference between the spin–orbit angular velocities vanishes at $t = 0$, $\Delta\Omega_{\text{SO}} \equiv \Omega_{\text{SO}}^{(2)} - \Omega_{\text{SO}}^{(1.5)} = 0$, and is therefore initially negligible compared to the secular spin–spin contribution $\bar{\Omega}_{\text{SS}}$ retained in Eq. (D.8). The relevant question is thus to determine the timescale over which $\Delta\Omega_{\text{SO}}$ could grow and potentially become comparable to $\bar{\Omega}_{\text{SS}}$.

By an argument analogous to that leading to Eq. (D.9), the difference between the orbital variables \mathbf{l} and \mathbf{r} predicted by the two models grows linearly with time and satisfies

$$\Delta\mathbf{l}(t), \Delta\mathbf{r}(t) = \mathcal{O}(t c^{-4}). \quad (\text{D.14})$$

The difference between the spin–orbit terms can be then estimated as

$$\Omega_{\text{SO}}^{(2)}(t) - \Omega_{\text{SO}}^{(1.5)}(t) = \frac{\delta_1}{c^2} \left(\frac{\mathbf{l}^{(2)}}{r^{3(2)}} - \frac{\mathbf{l}^{(1.5)}}{r^{3(1.5)}} \right) = \mathcal{O}(t c^{-6}). \quad (\text{D.15})$$

Substituting this estimate into the general bound (D.6) shows that the cumulative contribution of $\Delta\Omega_{\text{SO}}$ to the spin error scales as

$$\|\mathbf{s}_1^{(2)} - \mathbf{s}_1^{(1.5)}\|_{\text{SO}} = \mathcal{O}\left(s_1 \int_0^t \|\Delta\Omega_{\text{SO}}(\tau)\| d\tau\right) = \mathcal{O}(t^2 c^{-7}). \quad (\text{D.16})$$

For times $t \lesssim \mathcal{O}(c^3)$, this contribution is therefore subdominant compared to the linear in time $\mathcal{O}(t c^{-4})$ error induced by the missing secular spin–spin term. Consequently, neglecting $\Delta\Omega_{\text{SO}}$ is fully justified for $t \lesssim \mathcal{O}(c^3) \sim \mathcal{O}(\tau_{\text{prec}}^{3/2})$, which is the regime of interest in our work.

An analogous analysis can be carried out for the remaining bounds, given by Eqs. (D.11) and (D.13), and leads to the same conclusion: the corrections induced by the missing model labels in $\Delta\Omega_{\text{SO}}$ are always subdominant, over the timescales of interest, compared to the contributions governed by $\tilde{\Omega}_{\text{SO}}$ and $\tilde{\Omega}_{\text{SS}}$, respectively.

Appendix E: Polynomial form of p_r^2

The coefficients appearing in Eq. (4.3) depend solely on h , l , and the spins. They are given explicitly by

$$\tilde{A} = 2h + \frac{1}{c^2} (1 - 3\nu)h^2 - \frac{1}{c^4} \nu(1 - 4\nu)h^3, \quad (\text{E.1a})$$

$$\tilde{B} = 1 + \frac{1}{c^2} (4 - \nu)h + \frac{1}{c^4} (2 - 2\nu + \nu^2)h^2, \quad (\text{E.1b})$$

$$\tilde{C} = -l^2 + \frac{1}{c^2} (6 + \nu) + \frac{1}{c^4} 15h, \quad (\text{E.1c})$$

$$\tilde{D}_1 = -\frac{1}{c^2} [\nu l^2 + 2\mathbf{l} \cdot \mathbf{s}_{\text{eff}} - \mathbf{S}^2 + 3(\mathbf{n} \cdot \mathbf{S})^2] + \frac{1}{c^4} \left[\frac{17}{2} + \frac{5\nu}{2} + 2\nu^2 - \nu(1 + \nu)hl^2 \right], \quad (\text{E.1d})$$

$$\tilde{D}_2 = -\frac{1}{c^4} \nu(1 + 3\nu)l^2, \quad (\text{E.1e})$$

$$\tilde{D}_3 = \frac{1}{c^4} \frac{3\nu^2}{4} l^4. \quad (\text{E.1f})$$

Appendix F: Equation of motion of \mathbf{R}

The equation of motion for \mathbf{R} can be obtained in two equivalent ways: either by computing its Poisson bracket with the Hamiltonian, or by directly applying Hamilton's equations

$$\begin{aligned} \frac{d\mathbf{r}}{dt} &= \frac{\partial H}{\partial \mathbf{p}}, \\ &= \mathbf{p} - \frac{1}{2c^2} \left[(1 - 3\nu)p^2 \mathbf{p} + \frac{2}{r} \left((3 + \nu)\mathbf{p} + \nu(\mathbf{n} \cdot \mathbf{p})\mathbf{n} \right) + \frac{2}{r^2} (\mathbf{n} \times \mathbf{s}_{\text{eff}}) \right] \\ &\quad + \frac{1}{8c^4} \left[3(1 - 5\nu + 5\nu^2)p^4 \mathbf{p} + \frac{4}{r} \left((5 - 20\nu - 3\nu^2)p^2 \mathbf{p} - \nu^2((\mathbf{n} \cdot \mathbf{p})p^2 \mathbf{n} + (\mathbf{n} \cdot \mathbf{p})^2 \mathbf{p} - 3(\mathbf{n} \cdot \mathbf{p})^3 \mathbf{n}) \right) \right. \\ &\quad \left. + \frac{8}{r^2} \left((5 + 8\nu)\mathbf{p} + 3\nu(\mathbf{n} \cdot \mathbf{p})\mathbf{n} \right) \right]. \end{aligned} \quad (\text{F.1})$$

Appendix G: Justification of the quasi-Keplerian ansatz

In this appendix, we justify the functional form of the quasi-Keplerian parametrization used in Sec. 4C by analyzing the harmonic content of the equations of motion to determine the minimal set of oscillatory corrections required at 2PN order with spins.

1. Harmonic analysis of the radial equation

The radial equation of motion (4.4) reads

$$\left(\frac{dr}{dt} \right)^2 = A + \frac{2B}{r} + \frac{C}{r^2} + \frac{D_1}{r^3} + \frac{D_2}{r^4} + \frac{D_3}{r^5}, \quad (\text{G.1})$$

where $D_1 = D_{1o} + D_{1s}$. Time-dependent 2PN spin corrections arise from oscillating terms in C and D_{1s} . Substituting the expressions from Eq. (4.16) and using $\phi = v_\phi$ and $r = a(1 - e^2)/(1 + e \cos v_\phi)$ at Newtonian order, these oscillatory contributions take the form

$$\Delta_r = \frac{1}{c^4} \sum_{k=0}^5 \left[a_k^{(r)} \cos(kv_\phi - 2\phi_s) + b_k^{(r)} \sin(kv_\phi - 2\phi_s) \right], \quad (\text{G.2})$$

where the coefficients $a_k^{(r)}$ and $b_k^{(r)}$ depend on the orbital and spin parameters. The harmonic expansion terminates at $k = 5$ because C contains up to 3 harmonics while r^{-2} contributes to 2, and similarly D_{1s} has 2 harmonics while r^{-3} contributes to 3.

To reproduce these harmonics on the left-hand side without generating unnecessary higher harmonics, we construct the quasi-Keplerian parametrization perturbatively around the 2PN non-spinning solution plus the 1.5PN dynamics

$$n(t - t_0) = u - e_t \sin u + \frac{1}{c^4} [f_t \sin v_\phi + g_t(v_\phi - u)], \quad (\text{G.3a})$$

$$r = a_r(1 - e_r \cos u), \quad (\text{G.3b})$$

$$v_\phi = u + 2 \arctan \left(\frac{\beta_\phi \sin u}{1 - \beta_\phi \cos u} \right), \quad \beta_\phi = \frac{e_\phi}{1 + \sqrt{1 - e_\phi^2}}. \quad (\text{G.3c})$$

We then add 2PN spin corrections

$$r \rightarrow a_r(1 - e_r \cos u) + \frac{1}{c^4} \sum_{m=1}^M h_r^{(m)} \cos(mv_\phi - 2\phi_s), \quad (\text{G.4a})$$

$$n(t - t_0) \rightarrow u - e_t \sin u + \frac{1}{c^4} \left[f_t \sin v_\phi + g_t(v_\phi - u) + \sum_{n=1}^N h_t^{(n)} \sin(nv_\phi - 2\phi_s) \right], \quad (\text{G.4b})$$

where $h_r^{(m)}$ and $h_t^{(n)}$ are constant coefficients on the orbital timescale. Using the chain rule

$$\left(\frac{dr}{dt} \right)^2 = \left(\frac{dr}{dv_\phi} \right)^2 \left(\frac{dv_\phi}{dt} \right)^{-2}, \quad (\text{G.5})$$

and requiring no harmonics beyond $k = 5$, we find $m \leq 2$ and $n \leq 1$

$$r = a_r(1 - e_r \cos u) + \frac{1}{c^4} \left[h_r^{(1)} \cos(v_\phi - 2\phi_s) + h_r^{(2)} \cos(2v_\phi - 2\phi_s) \right], \quad (\text{G.6a})$$

$$n(t - t_0) = u - e_t \sin u + \frac{1}{c^4} \left[f_t \sin v_\phi + g_t(v_\phi - u) + h_t^{(1)} \sin(v_\phi - 2\phi_s) \right]. \quad (\text{G.6b})$$

2. Harmonic analysis of the azimuthal equation

The azimuthal equation of motion (4.23), omitting the last term that we treat separately, reads

$$r^2 \frac{d\phi}{dt} = F + \frac{I_1}{r} + \frac{I_2}{r^2} + \frac{I_3}{r^3}. \quad (\text{G.7})$$

Following the same analysis, the oscillatory 2PN spin contributions are

$$\Delta_\phi = \frac{1}{c^4} \sum_{k=0}^3 \left[a_k^{(\phi)} \cos(kv_\phi - 2\phi_s) + b_k^{(\phi)} \sin(kv_\phi - 2\phi_s) \right], \quad (\text{G.8})$$

where the expansion terminates at $k = 3$ due solely to oscillations of l^2 in F . We parametrize

$$\phi - \phi_0 = (1 + \tilde{k})v_\phi + \frac{1}{c^4} \left[f_\phi \sin 2v_\phi + g_\phi \sin 3v_\phi + \sum_{\ell=1}^L h_\phi^{(\ell)} \sin(\ell v_\phi - 2\phi_s) \right]. \quad (\text{G.9})$$

Computing $d\phi/dt$ via the chain rule and verifying consistency with the radial constraints ($m \leq 2$, $n \leq 1$) yields $\ell \leq 3$.

3. Complete quasi-Keplerian parametrization

The harmonic analysis of both equations yields the following minimal ansatz for the complete quasi-Keplerian parametrization of the relative separation vector \mathbf{R}

$$n(t - t_0) = u - e_t \sin u + \frac{1}{c^4} \left[f_t \sin v_\phi + g_t(v_\phi - u) + h_t \sin(v_\phi - 2\phi_s) \right], \quad (\text{G.10a})$$

$$r = a_r(1 - e_r \cos u) + \frac{1}{c^4} \left[h_{r1} \cos(v_\phi - 2\phi_s) + h_{r2} \cos(2v_\phi - 2\phi_s) \right], \quad (\text{G.10b})$$

$$\begin{aligned} \phi - \phi_0 = (1 + \tilde{k})v_\phi + \frac{1}{c^4} & \left[f_\phi \sin 2v_\phi + g_\phi \sin 3v_\phi \right. \\ & \left. + h_{\phi1} \sin(v_\phi - 2\phi_s) + h_{\phi2} \sin(2v_\phi - 2\phi_s) + h_{\phi3} \sin(3v_\phi - 2\phi_s) \right]. \end{aligned} \quad (\text{G.10c})$$

This minimal parametrization contains the fewest harmonic corrections necessary to represent the 2PN spin dynamics and recovers the same functional structure as the ansatz introduced by Klein and Jetzer [Eqs. (A1)–(A4), Ref. [42]]. The spin-dependent coefficients h_t , h_{r1} , h_{r2} , $h_{\phi1}$, $h_{\phi2}$, $h_{\phi3}$, together with the 2PN corrections to the existing quasi-Keplerian

parameters $(n, a_r, e_r, e_t, e_\phi, \tilde{k}, f_t, g_t, f_\phi, g_\phi)$, are determined by substituting Eqs. (G.10) into the equations of motion and requiring both to be satisfied identically. This procedure yields the solution presented in Eqs. (4.25) and (4.27).

Appendix H: The spin-aligned limit

In this appendix, we demonstrate that our general 2PN spinning quasi-Keplerian parametrization smoothly recovers the standard results for aligned-spin eccentric binary black holes (e.g., Refs. [27, 54]).

In the spin-aligned configuration, both spin vectors align completely with the orbital angular momentum. This alignment dictates that the relative spin angles $\kappa_1, \kappa_2, \gamma$ vanish, along with the in-plane amplitude s_p of the mass-weighted spin vector \mathcal{S} . This is a direct consequence of the orbital angular momentum vector \mathbf{L} remaining strictly constant in this limit. Both spin vectors are permanently orthogonal to the orbital plane, maintaining strict orthogonality with the relative separation vector \mathbf{R} and the momentum vector \mathbf{P} (Eq. (4.7b)).

The orbital equation of motion Eq. (4.4) is perfectly regular in the spin-aligned limit. Consequently, we can evaluate this limit directly on the general integrated solutions provided in Eqs. (4.25a) and (4.25b). Because the coefficient h_r is strictly proportional to s_p^2 , the 2PN oscillatory spin corrections associated with precession inherently vanish as $s_p \rightarrow 0$. By taking this limit, the general radial and temporal quasi-Keplerian parameters $(n, a_r, e_t, e_r, f_t, g_t)$ in Eq. (4.27) identically reduce to those derived in Ref. [27] without requiring further mathematical manipulation.

The azimuthal sector, however, demands a more careful treatment. We cannot directly compare the non-inertial phase $\phi(t)$ from Eq. (4.25d) to the inertial phase parameters $(k, e_\phi, f_\phi, g_\phi)$ established in the aligned-spin literature. We must first project the orbital phase into the inertial frame.

Our generic parametrization tracks the binary's position in the non-inertial frame (NIF), where the orbit is instantaneously confined to the ij -plane

$$\mathbf{r}_{\text{NIF}} = r \begin{bmatrix} \cos \phi \\ \sin \phi \\ 0 \end{bmatrix}. \quad (\text{H.1})$$

To determine the true physical position observed in the fixed inertial frame (IF) utilized by the aligned-spin literature, we apply the inverse Euler rotation $\Lambda_{\text{NIF} \rightarrow \text{IF}} = \Lambda_{\text{IF} \rightarrow \text{NIF}}^T$ to \mathbf{r}_{NIF} . In the aligned-spin configuration, the orbital angular momentum does not precess, and the inclination strictly vanishes ($\theta_L \rightarrow 0$). To smoothly map the non-inertial coordinates to the inertial frame, we expand the transformation for a small inclination angle $\theta_L \ll 1$. This yields for the relative separation

$$\mathbf{r}_{\text{IF}} = r \begin{bmatrix} \cos \phi_L \cos \phi - \sin \phi_L (1 - \mathcal{O}(\theta_L^2)) \sin \phi \\ \sin \phi_L \cos \phi + \cos \phi_L (1 - \mathcal{O}(\theta_L^2)) \sin \phi \\ \mathcal{O}(\theta_L) \end{bmatrix} = r \begin{bmatrix} \cos(\phi + \phi_L) \\ \sin(\phi + \phi_L) \\ 0 \end{bmatrix} + \mathcal{O}(\theta_L). \quad (\text{H.2})$$

Because these $\mathcal{O}(\theta_L)$ corrections can be chosen beyond the 2PN order, they trivially decouple from the dynamics. Taking the exact limit $\theta_L \rightarrow 0$ safely drops these terms, leaving the physical configuration perfectly well-posed and demonstrating that the true inertial phase is simply $\Phi_{\text{spin-aligned}} = \phi + \phi_L$.

To recover the aligned-spin azimuthal quasi-Keplerian parameters, we evaluate the limit directly on the integrated phase solutions given in Eq. (3.29) (modified with the hybrid description) and Eq. (4.25d).

In the strict aligned-spin limit ($\kappa_1 \rightarrow 0$), the precession amplitude vanishes, and the incomplete elliptic integrals reduce into the purely orbital hybrid anomaly $\Upsilon^{(2,\text{H})}$. Noting that the terms proportional to β_{2L} cancel exactly, we can sum the phase components to obtain

$$\Phi_{\text{spin-aligned}}(v_\phi, v_r, u) = (1 + \tilde{k})v_\phi + \frac{1}{c^4} [f_\phi \sin 2v_\phi + g_\phi \sin 3v_\phi] + \frac{3(1 - \lambda)(l + \mathcal{S}) + \nu(l + s_1 + s_2)}{\sqrt{A(x_3 - x_-)}} \Upsilon^{(2,\text{H})}(v_r, u). \quad (\text{H.3})$$

To express the orbital phase entirely in terms of single true anomaly v_θ , the eccentric anomaly u appearing in $\Upsilon^{(2,\text{H})}$ is first converted to the radial true anomaly v_r using the identities

$$\frac{\sin u}{1 - e_r \cos u} = \frac{\sin v_r}{\sqrt{1 - e_r^2}}, \quad (\text{H.4})$$

$$\frac{\sin u}{(1 - e_r \cos u)^2} = \frac{\sin v_r}{(1 - e_r^2)^{3/2}} + \frac{e_r \sin(2v_r)}{2(1 - e_r^2)^{3/2}}. \quad (\text{H.5})$$

The orbital phase then assumes the general harmonic form

$$\Phi_{\text{spin-aligned}}(v_\phi, v_r) = A_0 v_\phi + B_0 v_r + B_1 \sin v_r + A_2 \sin(2v_\phi) + B_2 \sin(2v_r) + A_3 \sin(3v_\phi), \quad (\text{H.6})$$

where the coefficients A_i and B_i are functions of h, l, s_1 , and s_2 .

To express the orbital phase in terms of a single true anomaly, we must map v_r to v_ϕ . Because the eccentricities e_r and e_ϕ differ starting at the 1PN order, this mapping requires an anomaly shift. For any two true anomalies v_{old} and v_{new} whose corresponding eccentricities share the same Newtonian order and relate via

$$e_{\text{new}} = e_{\text{old}} \left(1 + \frac{N_2}{c^2} + \frac{N_3}{c^3} + \frac{N_4}{c^4} \right), \quad (\text{H.7})$$

the perturbative expansion relating the two anomalies up to the 2PN order is given by

$$v_{\text{old}} = v_{\text{new}} - \frac{e_{\text{old}}}{1 - e_{\text{old}}^2} \left(\frac{N_2}{c^2} + \frac{N_3}{c^3} \right) \sin v_{\text{new}} - \frac{1}{c^4} \left[\left(N_4 + \frac{N_2^2 e_{\text{old}}^2}{1 - e_{\text{old}}^2} \right) \frac{e_{\text{old}} \sin v_{\text{new}}}{1 - e_{\text{old}}^2} - \frac{N_2^2 e_{\text{old}}^2}{4(1 - e_{\text{old}}^2)^2} \sin(2v_{\text{new}}) \right]. \quad (\text{H.8})$$

By applying this shift with $v_{\text{old}} = v_r$ and $v_{\text{new}} = v_\phi$, we can write the phase entirely as a function of v_ϕ

$$\Phi_{\text{spin-aligned}}(v_\phi) = C_0 v_\phi + C_1 \sin v_\phi + C_2 \sin(2v_\phi) + C_3 \sin(3v_\phi), \quad (\text{H.9})$$

where the coefficients C_i are functions of h, l, s_1 , and s_2 .

Finally, in the standard quasi-Keplerian formalism, we require the first harmonic to be identically zero. To achieve this, we introduce the final true anomaly v_θ , characterized by an eccentricity e_θ . We apply the anomaly shift transformation once more (from v_ϕ to v_θ). The eccentricity e_θ is fixed precisely by demanding that the coefficient of $\sin v_\theta$ identically vanishes. After absorbing this harmonic and collecting all contributions, the phase reduces to the standard non-precessing form

$$\Phi_{\text{spin-aligned}}(v_\theta) = (1 + k_\theta)v_\theta + f_\theta \sin(2v_\theta) + g_\theta \sin(3v_\theta). \quad (\text{H.10})$$

Evaluating these coefficients in terms of our 2PN variables yields

$$k_\theta = \frac{1}{l^2 c^2} \left[3 - \frac{2\mathbf{l} \cdot \mathbf{s}_{\text{eff}}}{l^2} + \frac{3\mathcal{S}^2}{2l^2} \right] + \frac{1}{4l^4 c^4} [105 - 30\nu + 2(15 - 6\nu)hl^2], \quad (\text{H.11})$$

$$f_\theta = \frac{1}{c^4} \frac{\nu(1 - 3\nu)}{8l^4} (1 + 2hl^2), \quad (\text{H.12})$$

$$g_\theta = -\frac{1}{c^4} \frac{3\nu^2}{32l^4} (1 + 2hl^2)^{3/2}, \quad (\text{H.13})$$

$$e_\theta^2 = 1 + 2hl^2 - \frac{h}{c^2} \left[12 + (15 - \nu)hl^2 - \frac{8(1 + hl^2)\mathbf{l} \cdot \mathbf{s}_{\text{eff}}}{l^2} + \frac{2(3 + 4hl^2)\mathcal{S}^2}{l^2} \right] - \frac{h}{8l^2 c^4} [408 - 232\nu - 15\nu^2 + 4(16 - 88\nu - 9\nu^2)hl^2 - 4(160 - 30\nu + 3\nu^2)h^2 l^4]. \quad (\text{H.14})$$

These expressions perfectly reproduce the aligned-spin parameters derived in Ref. [27]. This demonstrates that integrating the precessing equations of motion first and subsequently taking the spin-aligned limit is a mathematically consistent and commuting procedure.

Appendix I: The Four Fundamental Frequencies of the 2PN Dynamics

In the action-angle formulation of the conservative binary black hole problem, the number of fundamental frequencies emerges directly from the dimensionality of the phase space and the symmetries of the Hamiltonian. The system is initially described by four vectors: the relative separation \mathbf{r} , the canonical momentum \mathbf{p} , and the two spin vectors \mathbf{s}_1 and \mathbf{s}_2 , yielding a 12-dimensional phase space. Under the NWP spin supplementary condition, the conservative dynamics strictly preserve the magnitudes of the individual spins, s_1 and s_2 . This constraint reduces the active phase space to 10 dimensions, which corresponds to 5 physical degrees of freedom. However, because the isolated binary system possesses global rotational invariance, the total angular momentum vector \mathbf{J} is strictly conserved. If we align

the inertial z -axis with \mathbf{J} , the action associated with J_z is a constant of motion. The rotational symmetry dictates that the Hamiltonian is independent of the global azimuthal angle conjugate to J_z , meaning its associated frequency strictly vanishes. This symmetry reduction removes one dynamical degree of freedom, leaving the 2PN spinning system with exactly four non-zero fundamental frequencies that govern its multi-timescale evolution.

The first two frequencies characterize the quasi-Keplerian orbital motion. The radial frequency, or mean motion n , governs the period of radial oscillation from periastron to periastron and is explicitly given in Eq. (4.27). As the eccentric anomaly u evolves from 0 to 2π , the orbital phase ϕ defined in Eq. (4.25d) changes by $(1+k)2\pi$. Consequently, the azimuthal frequency is given by $\omega_\phi = n(1+k)$, where k represents the effective periastron advance defined in Eq. (4.28).

The third frequency, ω_{nut} , governs the internal dynamics of the spin subsystem. While individual spin magnitudes are constant, spin-orbit and spin-spin interactions cause the relative angle between the spins ($\cos\gamma$) and their inclinations relative to the orbital angular momentum ($\cos\kappa_1, \cos\kappa_2$) to oscillate. The inclination of the orbital plane, θ_L , shares this same periodicity due to its dependence on the Σ_i parameters. This oscillation is captured by the single degree of freedom $\cos\kappa_1$, whose evolution is determined by the linear growth of the argument $\Upsilon(t)$. Since the $\text{sn}^2(\Upsilon, \beta)$ term in Eq. (3.19) has a period of $2K(\beta)$ relative to its argument, the physical nutation frequency evaluates to

$$\omega_{\text{nut}} = \frac{\pi\sqrt{A(x_3 - x_-)}}{4c^2d^3K(\beta)}, \quad (\text{I.1})$$

where $K(\beta)$ is the complete elliptic integral of the first kind, A is defined in Eq. (3.18), x_-, x_3 are the roots of the cubic polynomial detailed in Appendix B and d , defined in Eq. (3.8), depends on the 1PN QKP.

The fourth frequency, ω_{prec} , characterizes the period over which the azimuthal angle ϕ_L changes by 2π , representing a complete rotation of \mathbf{L} around the invariant total angular momentum \mathbf{J} . This effect is extracted by isolating the linear drift of the azimuthal angle $\phi_L(t)$ given in Eq. (3.29). Specifically, the incomplete elliptic integrals of the third kind, Π , contain a secular growth proportional to the complete elliptic integral $\Pi(n, \beta)$. The secular precession frequency evaluates to

$$\omega_{\text{prec}} = \frac{1}{c^2d^3} \left[\frac{\beta_{1L}}{\alpha_{1L} + x_-} \frac{\Pi(n_1, \beta)}{K(\beta)} - \frac{\beta_{2L}}{\alpha_{2L} + x_-} \frac{\Pi(n_2, \beta)}{K(\beta)} + \beta_{3L} \right], \quad (\text{I.2})$$

where the elliptic characteristics are $n_1 = \frac{x_- - x_+}{\alpha_{1L} + x_-}$ and $n_2 = \frac{x_- - x_+}{\alpha_{2L} + x_-}$, and the coefficients α_{iL} and β_{iL} are explicitly defined in Eq. (3.27).

In the spin-aligned limit, the nutation frequency ω_{nut} vanishes identically as the relative orientations of the angular momentum and spin vectors become stationary. In this regime, the distinction between the non-inertial and inertial azimuthal motions disappears; the periastron advance, previously described in Eq. (H.11), is recovered by the sum $k_\theta = k + \omega_{\text{prec}}/n$. Consequently, the spin-related oscillations vanish and the system reduces to the standard two-frequency dynamics characteristic of non-precessing orbits, defined entirely by the quasi-Keplerian radial and azimuthal motions.

-
- [1] M. Hannam, C. Hoy, J. E. Thompson, S. Fairhurst, V. Raymond, *et al.*, General-relativistic precession in a black-hole binary [10.1038/s41586-022-05212-z](https://arxiv.org/abs/2112.11300), [arXiv:2112.11300](https://arxiv.org/abs/2112.11300) [gr-qc].
 - [2] R. Abbott *et al.* (LIGO Scientific, Virgo), GW190412: Observation of a Binary-Black-Hole Coalescence with Asymmetric Masses, *Phys. Rev. D* **102**, 043015 (2020), [arXiv:2004.08342](https://arxiv.org/abs/2004.08342) [astro-ph.HE].
 - [3] I. M. Romero-Shaw, P. D. Lasky, E. Thrane, and J. C. Bustillo, GW190521: orbital eccentricity and signatures of dynamical formation in a binary black hole merger signal, *Astrophys. J. Lett.* **903**, L5 (2020), [arXiv:2009.04771](https://arxiv.org/abs/2009.04771) [astro-ph.HE].
 - [4] D. Gerosa and M. Fishbach, Hierarchical mergers of stellar-mass black holes and their gravitational-wave signatures, *Nature Astron.* **5**, 749 (2021), [arXiv:2105.03439](https://arxiv.org/abs/2105.03439) [astro-ph.HE].
 - [5] I. Mandel and A. Farmer, Merging stellar-mass binary black holes, *Phys. Rept.* **955**, 1 (2022), [arXiv:1806.05820](https://arxiv.org/abs/1806.05820) [astro-ph.HE].
 - [6] I. Romero-Shaw, J. Stegmann, H. Tagawa, D. Gerosa, J. Samsing, N. Gupte, and S. R. Green, GW200208_222617 as an eccentric black-hole binary merger: Properties and astrophysical implications, *Phys. Rev. D* **112**, 063052 (2025), [arXiv:2506.17105](https://arxiv.org/abs/2506.17105) [astro-ph.HE].
 - [7] I. M. Romero-Shaw, D. Gerosa, and N. Loutrel, Eccentricity or spin precession? distinguishing subdominant effects in gravitational-wave data, *Monthly Notices of the Royal Astronomical Society* **519**, 5352 (2023), <https://academic.oup.com/mnras/article-pdf/519/4/5352/50423218/stad031.pdf>.
 - [8] S. Tibrewal, A. Zimmerman, J. Lange, and D. Shoemaker, Misinterpreting Spin Precession as Orbital Eccentricity in Gravitational-Wave Signals, (2026), [arXiv:2601.02260](https://arxiv.org/abs/2601.02260) [gr-qc].

- [9] [994, L47 \(2025\)](#).
- [10] V. Baibhav, Inferring Eccentricity of Binary Black Holes from Spin-Orbit Misalignment, (2025), [arXiv:2512.22044 \[astro-ph.HE\]](#).
- [11] L. Lehner, Numerical relativity: a review, *Classical and Quantum Gravity* **18**, R25 (2001).
- [12] U. Sperhake, The numerical relativity breakthrough for binary black holes, *Classical and Quantum Gravity* **32**, 124011 (2015).
- [13] K. D. Kokkotas and B. G. Schmidt, Quasi-normal modes of stars and black holes, *Living Reviews in Relativity* **2**, 2 (1999).
- [14] E. Berti, V. Cardoso, and A. O. Starinets, Quasinormal modes of black holes and black branes, *Classical and Quantum Gravity* **26**, 163001 (2009).
- [15] L. Blanchet, Gravitational radiation from post-newtonian sources and inspiralling compact binaries, *Living reviews in relativity* **17**, 2 (2014).
- [16] A. Buonanno and T. Damour, Effective one-body approach to general relativistic two-body dynamics, *Physical Review D* **59**, 084006 (1999).
- [17] S. Khan, S. Husa, M. Hannam, F. Ohme, M. Pürrer, X. J. Forteza, and A. Bohé, Frequency-domain gravitational waves from nonprecessing black-hole binaries. ii. a phenomenological model for the advanced detector era, *Physical Review D* **93**, 044007 (2016).
- [18] P. Schmidt, M. Hannam, S. Husa, and P. Ajith, Tracking the precession of compact binaries from their gravitational-wave signal, *Phys. Rev. D* **84**, 024046 (2011), [arXiv:1012.2879 \[gr-qc\]](#).
- [19] P. Schmidt, M. Hannam, and S. Husa, Towards models of gravitational waveforms from generic binaries: A simple approximate mapping between precessing and non-precessing inspiral signals, *Phys. Rev. D* **86**, 104063 (2012), [arXiv:1207.3088 \[gr-qc\]](#).
- [20] M. Boyle, R. Owen, and H. P. Pfeiffer, A geometric approach to the precession of compact binaries, *Phys. Rev. D* **84**, 124011 (2011), [arXiv:1110.2965 \[gr-qc\]](#).
- [21] K. Chatziioannou, A. Klein, N. Yunes, and N. Cornish, Constructing gravitational waves from generic spin-precessing compact binary inspirals, *Physical Review D* **95**, 104004 (2017).
- [22] J. N. Arredondo, A. Klein, and N. Yunes, Efficient gravitational-wave model for fully-precessing and moderately eccentric, compact binary inspirals, *Phys. Rev. D* **110**, 044044 (2024), [arXiv:2402.06804 \[gr-qc\]](#).
- [23] G. Morras, G. Pratten, and P. Schmidt, Improved post-Newtonian waveform model for inspiralling precessing-eccentric compact binaries, *Phys. Rev. D* **111**, 084052 (2025), [arXiv:2502.03929 \[gr-qc\]](#).
- [24] T. Damour and N. Deruelle, General relativistic celestial mechanics of binary systems. i. the post-newtonian motion, *Annales de l'I.H.P. Physique théorique* **43**, 107 (1985).
- [25] T. Damour, P. Jaranowski, and G. Schäfer, Nonlocal-in-time action for the fourth post-newtonian conservative dynamics of two-body systems, *Physical Review D* **89**, 064058 (2014).
- [26] G. Cho, S. Tanay, A. Gopakumar, and H. M. Lee, Generalized quasi-keplerian solution for eccentric, nonspinning compact binaries at 4pn order and the associated inspiral-merger-ringdown waveform, *Physical Review D* **105**, 064010 (2022).
- [27] M. Tessmer, J. Hartung, and G. Schäfer, Motion and gravitational wave forms of eccentric compact binaries with orbital-angular-momentum-aligned spins under next-to-leading order in spin-orbit and leading order in spin (1)-spin (2) and spin-squared couplings, *Classical and Quantum Gravity* **27**, 165005 (2010).
- [28] M. Tessmer, J. Hartung, and G. Schäfer, Aligned spins: orbital elements, decaying orbits, and last stable circular orbit to high post-newtonian orders, *Classical and Quantum Gravity* **30**, 015007 (2013).
- [29] R. V. Wagoner and C. M. Will, Post-Newtonian gravitational radiation from orbiting point masses., *Astrophys. J.* **210**, 764 (1976).
- [30] G. Schäfer and N. Wex, Second post-newtonian motion of compact binaries, *Physics Letters A* **174**, 196 (1993).
- [31] R.-M. Memmesheimer, A. Gopakumar, and G. Schaefer, Third post-Newtonian accurate generalized quasi-Keplerian parametrization for compact binaries in eccentric orbits, *Phys. Rev. D* **70**, 104011 (2004), [arXiv:gr-qc/0407049](#).
- [32] G. Cho, S. Tanay, A. Gopakumar, and H. M. Lee, Generalized quasi-Keplerian solution for eccentric, nonspinning compact binaries at 4PN order and the associated inspiral-merger-ringdown waveform, *Phys. Rev. D* **105**, 064010 (2022), [arXiv:2110.09608 \[gr-qc\]](#).
- [33] R. Arnowitt, S. Deser, and C. W. Misner, Republication of: The dynamics of general relativity, *General Relativity and Gravitation* **40**, 1997-2027 (2008).
- [34] G. Cho and H. M. Lee, Analytic keplerian-type parametrization for general spinning compact binaries with leading order spin-orbit interactions, *Phys. Rev. D* **100**, 044046 (2019), [arXiv:1908.02927 \[gr-qc\]](#).
- [35] R. Samanta, S. Tanay, and L. C. Stein, Closed-form solutions of spinning, eccentric binary black holes at 1.5 post-newtonian order, *Phys. Rev. D* **108**, 124039 (2023), [arXiv:2210.01605 \[gr-qc\]](#).
- [36] J. D. Schnittman, Spin-orbit resonance and the evolution of compact binary systems, *Phys. Rev. D* **70**, 124020 (2004), [arXiv:astro-ph/0409174](#).
- [37] D. Gerosa, M. Kesden, R. O'Shaughnessy, A. Klein, E. Berti, U. Sperhake, and D. Trifirò, Precessional instability in binary black holes with aligned spins, *Phys. Rev. Lett.* **115**, 141102 (2015), [arXiv:1506.09116 \[gr-qc\]](#).
- [38] D. Gerosa, M. Kesden, U. Sperhake, E. Berti, and R. O'Shaughnessy, Multi-timescale analysis of phase transitions in precessing black-hole binaries, *Phys. Rev. D* **92**, 064016 (2015), [arXiv:1506.03492 \[gr-qc\]](#).
- [39] S. Tanay, L. C. Stein, and J. T. Gálvez Gherzi, Integrability of eccentric, spinning black hole binaries up to second post-Newtonian order, *Phys. Rev. D* **103**, 064066 (2021), [arXiv:2012.06586 \[gr-qc\]](#).
- [40] E. Racine, Analysis of spin precession in binary black hole systems including quadrupole-monopole interaction, *Phys. Rev. D* **78**, 044021 (2008), [arXiv:0803.1820 \[gr-qc\]](#).
- [41] L. A. Gergely, Spin spin effects in radiating compact binaries, *Phys. Rev. D* **61**, 024035 (2000), [arXiv:gr-qc/9911082](#).

- [42] A. Klein and P. Jetzer, Spin effects in the phasing of gravitational waves from binaries on eccentric orbits, *Physical Review D—Particles, Fields, Gravitation, and Cosmology* **81**, 124001 (2010).
- [43] L. E. Kidder, Coalescing binary systems of compact objects to (post) 5/2-newtonian order. v. spin effects, *Physical Review D* **52**, 821 (1995).
- [44] B. M. Barker and R. F. O’Connell, Nongeodesic motion in general relativity, *General Relativity and Gravitation* **5**, 539 (1974).
- [45] T. Colin, 2PN_BBH_solution.nb: Mathematica notebook for the analytical 2PN spinning, eccentric binary black hole solution, <https://github.com/sashwattanay/BBH-PN-Toolkit> (2026), file: 2PN_BBH_solution.nb.
- [46] M. H. L. Pryce, The mass-centre in the restricted theory of relativity and its connexion with the quantum theory of elementary particles, *Proceedings of the Royal Society of London. Series A. Mathematical and Physical Sciences* **195**, 62 (1948).
- [47] T. D. Newton and E. P. Wigner, Localized states for elementary systems, *Rev. Mod. Phys.* **21**, 400 (1949).
- [48] T. Damour, Coalescence of two spinning black holes: An effective one-body approach, *Phys. Rev. D* **64**, 124013 (2001).
- [49] M. D. Hartl and A. Buonanno, The Dynamics of precessing binary black holes using the post-Newtonian approximation, *Phys. Rev. D* **71**, 024027 (2005), [arXiv:gr-qc/0407091](https://arxiv.org/abs/gr-qc/0407091).
- [50] B. M. Barker, S. N. Gupta, and R. D. Haracz, One-Graviton Exchange Interaction of Elementary Particles, *Phys. Rev.* **149**, 1027 (1966).
- [51] B. M. Barker and R. F. O’Connell, Gravitational two-body problem with arbitrary masses, spins, and quadrupole moments, *Phys. Rev. D* **12**, 329 (1975).
- [52] J. Steinhoff, Canonical formulation of spin in general relativity, *Annalen Phys.* **523**, 296 (2011), [arXiv:1106.4203 \[gr-qc\]](https://arxiv.org/abs/1106.4203).
- [53] S. Tanay, L. C. Stein, and G. Cho, Action-angle variables of a binary black hole with arbitrary eccentricity, spins, and masses at 1.5 post-newtonian order, *Physical Review D* **107**, 103040 (2023).
- [54] Q. Henry and M. Khalil, Spin effects in gravitational waveforms and fluxes for binaries on eccentric orbits to the third post-Newtonian order, *Phys. Rev. D* **108**, 104016 (2023), [arXiv:2308.13606 \[gr-qc\]](https://arxiv.org/abs/2308.13606).